From Small Scale to Large Scale in the World of CO2 Reduction

Chandrashekar, S.

DOI
10.4233/uuid:ec741dab-3f94-4544-97b2-e457d8acf18a

Publication date
2022

Document Version
Final published version

Citation (APA)
Chandrashekar, S. (2022). *From Small Scale to Large Scale: in the World of CO2 Reduction*. [Dissertation (TU Delft), Delft University of Technology]. https://doi.org/10.4233/uuid:ec741dab-3f94-4544-97b2-e457d8acf18a

From Small Scale to Large Scale

In the World of CO_2 Reduction

Sanjana Chandrashekar

FROM SMALL SCALE TO LARGE SCALE

IN THE WORLD OF CO_2 REDUCTION

Dissertation

for the purpose of obtaining the degree of doctor
at Delft University of Technology,
by the authority of the Rector Magnificus prof. dr. ir. T.H.J.J. van der Hagen,
chair of the Board for Doctorates,
to be defended publicly on Tuesday, 6 September 2022 at 10:00 o'clock.

by

Sanjana CHANDRASHEKAR

Master of Science in Chemical Engineering,
Technical university of Delft, The Netherlands,
born in Kolar, India.

This dissertation is approved by the promoters.

Composition of the doctoral committee:

Rector Magnificus,	chairman
Prof. dr. W.A. Smith,	Delft University of Technology
Prof. dr. J.J.C Geerlings,	Delft University of Technology

Independent members:

Prof. dr. B. Dam	Delft University of Technology
Prof. dr. G. Mul,	University of Twente
Dr. W. van der Stam	University of Utrecht
Dr. S. Haussener,	École Polytechnique Fédérale de Lausanne
Prof. dr. J. Ruud van Ommen,	Delft University of Technology, reserve member

Other Members:

Dr. T. Burdyny,	Delft University of Technology

Keywords: Catalysts, CO_2 Reduction, Metal alloys, Cations, Membrane Electrode Assemblies.

Printed by: Ridder Print | www.ridderprint.nl

Front & Back: Acrylic on canvas by the author

ISBN 978-94-6384-368-3

An electronic version of this dissertation is available at
http://repository.tudelft.nl/.

In our time of disturbance and radical change, we are crossing a threshold, a portal, or an unseen bridge from one world to another.
It could be said that the bridge is either collapsing beneath us, or being made as we walk together, in the long twilight hours when one civilization gives way to another.

Ganeen Marie Haugen

CONTENTS

1

INTRODUCTION

1.0.1. DECADE OF ACTION

The United Nations has declared the years 2020 to 2030 as the Decade of Action. It represents a universal call of actively working towards ending poverty and ensuring that the planet is safe for all people to enjoy peace and prosperity. Seventeen Sustainable Development Goals (SDGs) (Figure 1) have been detailed to combat many of the challenges the world faces right now in order to achieve said peace and prosperity. They cover key aspects deemed to ensure a well-rounded lifestyle for everyone. From poverty to personal health to sustainable communities, these goals are to be undertaken not only by organizations but also by individuals.

Although each goal detailed by the SDGs tackles important challenges people are facing, many of the goals have the common theme of tackling the current climate crisis. In order to achieve carbon neutrality by 2050 more regulations need to be imposed, which is what the SDGs aim to initiate globally. Our economic system is based on infinite growth, where we have developed a system of constant production and waste. Our systems need to incorporate the ideologies of reuse and reduction during the early stages of production. Achieving this is not the individual job of the government, science or industry but all of them together. This theme persists through many of the SDGs as it is of great importance that we take care of our future generations. Our technologies and lifestyle need to start incorporating the mindset of infinite game[1] to ensure resources are still available for them.

1.0.2. SETTING UP A CYCLE

Humans have shown ingenuity towards using the sources available around us to resolve our day to day problems. Thomas Malthus predicted that as long as resources are available, human population will thrive and grow beyond the means of planet.[2] It is what we end up defining as resources that will make us a sustainable species and hopefully deter the Malthusian Theory. Incorporating ideologies of production to reuse will ensure long lasting industries and societies. Allowing also a much-needed paradigm shift in our

thought processes, which is to think of the repercussions of our actions and incorporate a circular practices into our lives.

Figure 1.1: The sustainable development goals as described by the UN.

One such cycle that can be set up is the CO_2 cycle. Although there already exists a natural CO_2 cycle,[3][4] the anthropological use of carbon based energy sources has been adding much more CO_2 to the atmosphere than what our ecosystems can absorb.[4] Constructing such a cycle is advantageous on two fronts. The rate of CO_2 production as a by-product of our industrial processes is much greater than our planets capacity to absorb it back. This implies that for a species so reliant on carbon based compound the excess CO_2 presents the unique opportunity for utility.[4] Secondly the excess CO_2 has been causing accelerated climate changes the likes of which have not been observed before and any reduction in its concentrations in the atmosphere will help mitigate a disastrous outcome.[4]

One such technology that can make use of the excess CO_2 and turn it back into chemicals and feedstock for industrial processes is the electrochemical conversion of CO_2 and water.[5] In this approach, it is possible to have renewable electricity drive the conversion of CO_2 to intermediates and products such as carbon monoxide, formic acid, ethanol and various other hydrocarbons. [6][7] Such a system works on a simple principle; CO_2 and water is fed to a cathode, which provides electrons for the reduction of CO_2, while the anode performs a simultaneous oxidation reaction (typically water oxidation

to oxygen), all encompassed in an electrochemical cell. The reduction of CO_2 contains a series of intermediate reactions, each typically performed as a proton-electron transfer (PET). The product selectivity is governed by both the equilibrium potential needed to form a given product, as well as the number of proton's and electron's needed to form the product (equilibrium reactions for major CO_2 reduction products shown in eq.1.1-1.5).[5]

$$CO_2 + H_2O + 2e^- \rightarrow CO + 2OH^- \text{ (\textbf{-0.52V vs SHE})} \tag{1.1}$$

$$CO_2 + 6H_2O + 8e^- \rightarrow CH_4 + 8OH^- \text{ (\textbf{-0.25V vs SHE})} \tag{1.2}$$

$$2CO_2 + 88H_2O + 12e^- \rightarrow C_2H_4 + 12OH^- \text{ (\textbf{-0.34V vs SHE})} \tag{1.3}$$

$$2CO_2 + 9H_2O + 12e^- \rightarrow C_2H_5OH + 12OH^- \text{ (\textbf{-0.33V vs SHE})} \tag{1.4}$$

$$3CO_2 + 13H_2O + 18e^- \rightarrow C_3H_7OH + 18OH^- \text{ (\textbf{-0.32V vs SHE})} \tag{1.5}$$

In order for the electrochemical reduction of CO_2 to be truly effective in successfully producing such value added products, a series of challenges must be overcome:[8]

1. The CO_2 molecule has a low solubility in water, which leads to low kinetics of CO_2 reduction reactions. This can be combated by using catalysts with high surface areas,[9] high pressure systems to increase the solubility of CO_2,[10] electrolytes that have an higher affinity to CO_2 or gas diffusion electrodes (GDE).

2. More often than not, the catalysts used are quick to deactivate (i.e. they decrease in activity/current density, or begin to favor hydrogen evolution over CO_2 reduction) during the reduction processes due to impurities and surface reconstruction.

3. The reduction of carbon dioxide and water produces a mixture of products.[9][11] Detecting and separating these products accurately will be an energy intensive downstream process, and thus improving selectivity towards individual products is essential.

It is clear that significant problems still plague the CO_2 electroreduction process. A number of factors such as catalyst composition and structure, cell design and electrolyte composition can be varied in order to design a well-functioning process.

Electrolyte

Changing the composition of the electrolyte produces subtle but eye-opening effects on the mechanism of CO_2 reduction. Lab scale systems typically use neutral pH $KHCO_3$ solutions as the electrolyte for CO_2 reduction. However, using electrolytes with varying pH has shown that an alkaline electrolyte encourages CO_2 dissolution and hence can enhance activity. The pH gradient between the bulk pH and the local pH at the catalyst surface affects not only CO_2 reduction but also hydrogen evolution, tailoring the product distribution of the process.[12] It has also become evident that the specific cations and anions used in the electrolyte also play a role in the conversion of CO_2.[12][13][14][15] Activity increases as one moves along the alkaline metal group from the small Li cations to the larger Cs cations, which have inversely large solvated radii. In addition,[16][17][18] different groups of anions too have varying effects on the selectivity of the reactions.[13][19] Various hypotheses have been put forth in order to truly

understand the role of ions in the activation and conversion of CO_2. It has been proposed that cations and their hydration shells (Figure 1.2) moderate the concentrations of reaction intermediates at the electric double layer (EDL).[18][19] Both ions are also thought to specifically adsorb onto the catalyst surface stabilizing key reaction intermediates.[15][20] However, a single theory is yet to be agreed upon on how electrolyte composition can be used to tune the product distribution over the catalyst to our needs.[12]

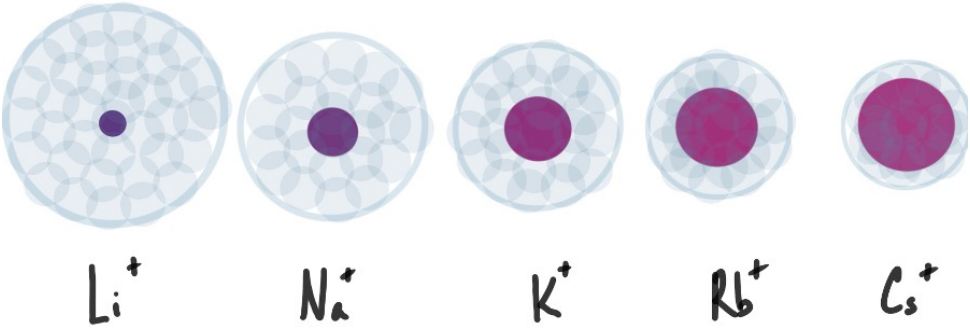

Figure 1.2: Schematic representation of the size of the alkaline earth metal cations and their hydration shells.[5][21]

CATALYST

The catalyst plays a central role in converting CO_2, and therefore understanding the electronic structure, composition, and defect structure of catalysts and their effect on the activity, selectivity, and stability for CO_2 electroreduction is vital. In order to take a process such as the electrochemical reduction of CO_2 from lab scale to industrial scale, the catalyst should be able to produce a single CO_2 reduction product with high selectivity and efficiency over a long period of operation. The distribution of products of the CO_2 conversion reactions on a particular catalyst depends on which of the transition and post-transition metals are used as the cathode during the process. These metals are hence grouped into four different categories based on the products they produce:

1. Carbon Monoxide
2. Hydrogen
3. Hydrocarbons
4. Formate/Formic Acid

From Figure 1.3, it can be seen that most metals produce H_2 (requiring 2 H^+/e^-) when placed in an aqueous environment and a negative potential is applied. Pt and Pd bind to CO with great affinity and poison themselves, not allowing further carbon dioxide

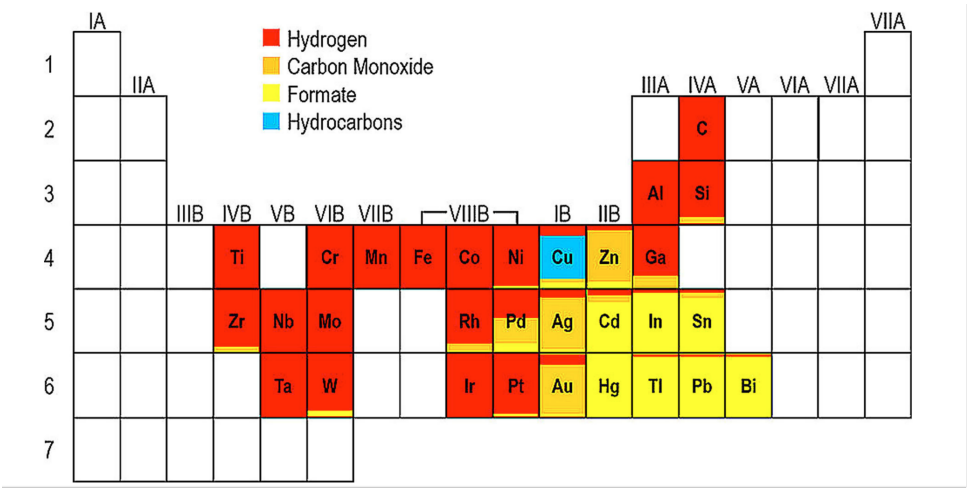

Figure 1.3: Periodic table showing the product distributions of CO_2 reduction reactions on the transition metals and other metals in 0.1M $KHCO_3$, based on data from Hori et. al

reduction. This is because the active sites required for carbon dioxide reduction are taken up by the strongly adsorbed carbon monoxide and the hydrogen evolution (HER) takes over.[22][23][24][25] Metals such as Au and Ag mainly produce CO from CO_2 (also needing 2 H^+/e^-), due to the weak binding strength of carbon monoxide to their surfaces.[25][26][27][28][29] Therefore, when the reaction proceeds from CO_2 to CO, CO desorbs easily and is not able to be further reduced/protonated to form higher order products. On the other hand, metals like Sn and Hg form a weak metal-carbon bond with carbon dioxide, and preferentially produce formic acid. The weak metal-carbon bond restricts the dissociation of the C-O bond.[30][31][32] Cu is a unique metal for CO_2 reduction as it possesses an intermediate binding strength to CO, which allows the ability for further reduction to higher value products, such as C2 and C3 species.[8][33][34][29]

It follows from this brief overview that there exists a relationship between the metal used as catalyst and the product it forms due to the different binding energies of the reaction intermediates on the surface. Gaining control over the way carbon dioxide reduction intermediates interact with the catalyst surface will help gain control over catalytic activities and final product distribution. It is possible to do this by making alloys of various metals,[35][36][37] in order to obtain intermediate binding energies that allow favorable pathways to a selected product. It may also be possible to change the local atomic structure of the catalysts to expose specific active sites at which certain reactions are known to occur.[38][39][40] This has been done with considerable success in lab scale electrochemical cells, as many structure-functionality relationships have been discovered over the past decades. Hence the catalyst provides another tool with which we can tune the conversion of CO_2 to different selective products

CELL ARCHITECTURE

As a crucial next step in the development of CO_2 reduction these catalysts will have to be tested at high current densities. This is because the transition from lab scale testing to industrial scales involves changes to the architecture of the electrochemical cell. For example, in order to reach high current densities, the low solubility of CO_2 will have to counteracted by using GDEs. GDEs are porous substrates onto which catalysts are deposited. They allow for pure CO_2 to reach the catalyst surface directly without any need for dissolution. They act as a physical barrier between the gaseous CO_2 and the electrolyte and is hence the location of the electrolyte – catalyst interface where reactions take place.[41]

The use of gaseous CO_2 in the reactor means that there will be a high concentration of CO_2, CO_2 reduction products and hydrogen at the cathode surface.[42] Large concentrations of CO_2 in contact with highly alkaline media will produce carbonates and bicarbonates which will precipitate out as salts upon the interaction with cations (discussed in detail in Chapter 4). Different products of CO_2 reduction can also interact with the catalyst (as their residence times in the reactor are much longer compared to lab scale systems).

Moving to high current densities will also imply large ohmic losses between the electrodes if liquid electrolytes are used. This is counteracted by using solid electrolytes such as Proton Exchange Membranes (PEMs) or Anion Exchange Membranes (AEMs). If the two electrodes are then sandwiched together without a flowing liquid catholyte, a membrane electrode assembly (MEA) is formed, with the membrane helping reduce ohmic losses in the system. This complicates the electrolyte-catalyst interface further as the effects of the monomers used in these membranes on the reaction mechanism is still not completely understood.

Hence architectural changes will lead to reaction conditions that are not necessarily similar to lab scale architectures. Testing alloys in high current density cells such as GDEs and MEAs will help us understand if catalytic activity translates directly from small scale to large scales. This will provide further understanding of how such changes to the architecture of the cell will affect the local reaction environment at the cathode.

1.0.3. THESIS OUTLINE

This thesis due to curious circumstances, that are not uncommon to a doctorate program, includes studies done on three different scales.

- What role does the electrolyte cation play during CO_2 reduction?
- How does mixing Au and Sn with varying ratios affect the product selectivity of CO_2 reduction compared to the individual components?
- How does using one of the best reported alloys for CO production in an aqueous environment translate to an MEA configuration?

These questions are specifically answered in Chapters 2,3 and 4 respectively. Chapter 2 is a fundamental study, where we use in situ surface enhanced infra-red absorption spectroscopy (SEIRAS) to probe reaction intermediates as a function of cation concentration. Chapter 3 consists of a lab scale study where we study AuSn bimetallic systems and how

catalytic activity depends on the structure and composition of the catalyst. And finally, in Chapter 4, we test AgPd alloys in a MEA configuration at industrially relevant scales and compare the activity and selectivity to previously reported systems operating in an aqueous H-cell environment.

BIBLIOGRAPHY

[1] Simon Sinek. *The Infinite Game*.

[2] Thomas Malthus. *An Essay on the Principle of Population*. 1798.

[3] Tom J. Battin et al. "The boundless carbon cycle". In: *Nature Geoscience* 2.9 (2009), pp. 598–600. ISSN: 17520894. DOI: 10.1038/ngeo618.

[4] Piers J. Sellers et al. "Observing carbon cycle–climate feedbacks from space". In: *Proceedings of the National Academy of Sciences of the United States of America* 115.31 (2018), pp. 7860–7868. ISSN: 10916490. DOI: 10.1073/pnas.1716613115.

[5] Y. Hori. "Electrochemical CO2 Reduction on Metal Electrodes". In: *Modern Aspects of Electrochemistry*. Ed. by Constantinos G. Vayenas, Ralph E. White, and Maria E. Gamboa-Aldeco. New York, NY: Springer New York, 2008, pp. 89–189. ISBN: 978-0-387-49489-0. DOI: 10.1007/978-0-387-49489-0_3. URL: https://doi.org/10.1007/978-0-387-49489-0_3.

[6] Evgenii V. Kondratenko et al. "Status and perspectives of CO2conversion into fuels and chemicals by catalytic, photocatalytic and electrocatalytic processes". In: *Energy and Environmental Science* 6.11 (2013), pp. 3112–3135. ISSN: 17545692. DOI: 10.1039/c3ee41272e.

[7] IPCC et al. *Climate Change 2021: The Physical Science Basis. Contribution of Working Group I to the Sixth Assessment Report of the Intergovernmental Panel on Climate Change*. Tech. rep. In Press. 2021, In Press. URL: https://www.ipcc.ch/report/ar6/wg1/.

[8] Mulatu Kassie Birhanu et al. "Copper and Copper-Based Bimetallic Catalysts for Carbon Dioxide Electroreduction". In: *Advanced Materials Interfaces* 1800919 (2018), pp. 1–34. ISSN: 21967350. DOI: 10.1002/admi.201800919.

[9] Qi Lu et al. "A selective and efficient electrocatalyst for carbon dioxide reduction". In: *Nature Communications* 5 (2014), pp. 1–6. ISSN: 20411723. DOI: 10.1038/ncomms4242. arXiv: arXiv:1011.1669v3.

[10] Min Liu et al. "Enhanced electrocatalytic CO2 reduction via field-induced reagent concentration". In: *Nature* 537.7620 (2016), pp. 382–386. ISSN: 14764687. DOI: 10.1038/nature19060. URL: http://dx.doi.org/10.1038/nature19060.

[11] Dong Dong Zhu, Jin Long Liu, and Shi Zhang Qiao. "Recent Advances in Inorganic Heterogeneous Electrocatalysts for Reduction of Carbon Dioxide". In: *Advanced Materials* 28.18 (2016), pp. 3423–3452. ISSN: 15214095. DOI: 10.1002/adma.201504766.

[12] Marilia Moura de Salles Pupo and Ruud Kortlever. "Electrolyte Effects on the Electrochemical Reduction of CO2". In: *ChemPhysChem* 20.22 (2019), pp. 2926–2935. ISSN: 14397641. DOI: 10.1002/cphc.201900680.

[13] Joaquin Resasco et al. “Promoter Effects of Alkali Metal Cations on the Electrochemical Reduction of Carbon Dioxide”. In: *Journal of the American Chemical Society* 139.32 (2017). ISSN: 15205126. DOI: 10.1021/jacs.7b06765.

[14] Meenesh R. Singh et al. “Hydrolysis of Electrolyte Cations Enhances the Electrochemical Reduction of CO2 over Ag and Cu”. In: *Journal of the American Chemical Society* 138.39 (2016), pp. 13006–13012. ISSN: 15205126. DOI: 10.1021/jacs.6b07612.

[15] Matthias M. Waegele et al. “How cations affect the electric double layer and the rates and selectivity of electrocatalytic processes”. In: *Journal of Chemical Physics* 151.16 (2019). ISSN: 00219606. DOI: 10.1063/1.5124878. URL: https://doi.org/10.1063/1.5124878.

[16] Sohail Anjum Shahzad. “Carbon Monoxide Adsorption on Copper and Silver Electrodes during Carbon Dioxide Electroreduction Studied by Infrared Reflection Absorption Spectroscopy and Surface-Enhanced Raman Spectroscopy”. In: *Langmuir* 12.4 (1996), pp. 1094–1097. DOI: 10.1007/978-3-642-33173-2_5.

[17] Michael R. Thorson, Karl I. Siil, and Paul J.A. Kenis. “Effect of cations on the electrochemical conversion of CO2 to CO”. In: *Journal of the Electrochemical Society* 160.1 (2013). ISSN: 00134651. DOI: 10.1149/2.052301jes.

[18] Stefan Ringe et al. “Understanding cation effects in electrochemical CO2 reduction”. In: *Energy and Environmental Science* 12.10 (2019), pp. 3001–3014. ISSN: 17545706. DOI: 10.1039/c9ee01341e.

[19] Sun Hee Yoon et al. “Theoretical insight into effect of cation–anion pairs on CO2 reduction on bismuth electrocatalysts”. In: *Applied Surface Science* 532 (Dec. 2020), p. 147459. DOI: 10.1016/j.apsusc.2020.147459.

[20] A. N. Frumkin. “Influence of cation adsorption on the kinetics of electrode processes”. In: *Transactions of the Faraday Society* 55.1 (1959), pp. 156–167. ISSN: 00147672. DOI: 10.1039/tf9595500156.

[21] James E. Pander et al. “Understanding the Heterogeneous Electrocatalytic Reduction of Carbon Dioxide on Oxide-Derived Catalysts”. In: *ChemElectroChem* 5.2 (2018), pp. 219–237. ISSN: 21960216. DOI: 10.1002/celc.201701100.

[22] Marek Gajdoš, Andreas Eichler, and Jürgen Hafner. “CO adsorption on close-packed transition and noble metal surfaces: Trends from ab initio calculations”. In: *Journal of Physics Condensed Matter* 16.8 (2004), pp. 1141–1164. ISSN: 09538984. DOI: 10.1088/0953-8984/16/8/001. arXiv: 0401095 [cond-mat].

[23] J. K. Norskov et al. “Density functional theory in surface chemistry and catalysis”. In: *Proceedings of the National Academy of Sciences* 108.3 (2011), pp. 937–943. ISSN: 0027-8424. DOI: 10.1073/pnas.1006652108.

[24] W. H. Burrows, M. G. T. and Stockmayer. *The poisoning of a palladium catalyst by carbon monoxide*. 1940. DOI: 10.1098/rspa.1940.0101.

[25] Ming Ma et al. “Electrochemical Reduction of CO 2 on Compositionally Variant Au-Pt Bimetallic Thin Films”. In: *Nano Energy* 42.September (2017), pp. 51–57. ISSN: 22112855. DOI: 10.1016/j.nanoen.2017.09.043. URL: http://linkinghub.elsevier.com/retrieve/pii/S2211285517305827.

[26] Paramaconi Rodriguez and Marc T.M. Koper. “Electrocatalysis on gold”. In: *Physical Chemistry Chemical Physics* 16.27 (2014), pp. 13583–13594. ISSN: 14639076. DOI: 10.1039/c4cp00394b.

[27] Haeri Kim et al. “Surface-Morphology-Dependent Electrolyte Effects on Gold-Catalyzed Electrochemical CO2 Reduction”. In: *Journal of Physical Chemistry C* 121.41 (2017), pp. 22637–22643. ISSN: 19327455. DOI: 10.1021/acs.jpcc.7b06286.

[28] Shuo Zhao, Renxi Jin, and Rongchao Jin. “Opportunities and Challenges in CO2 Reduction by Gold- and Silver-Based Electrocatalysts: From Bulk Metals to Nanoparticles and Atomically Precise Nanoclusters”. In: *ACS Energy Letters* 3.2 (2018), pp. 452–462. ISSN: 23808195. DOI: 10.1021/acsenergylett.7b01104.

[29] Ming Ma et al. “Selective and Efficient Reduction of Carbon Dioxide to Carbon Monoxide on Oxide-Derived Nanostructured Silver Electrocatalysts”. In: *Angewandte Chemie - International Edition* 55.33 (2016), pp. 9748–9752. ISSN: 15213773. DOI: 10.1002/anie.201604654.

[30] Maor F. Baruch et al. “Mechanistic Insights into the Reduction of CO ₂ on Tin Electrodes using in Situ ATR-IR Spectroscopy”. In: *ACS Catalysis* 5.5 (2015), pp. 3148–3156. ISSN: 2155-5435. DOI: 10.1021/acscatal.5b00402. URL: http://pubs.acs.org/doi/10.1021/acscatal.5b00402.

[31] K. L. Womer and B. Kaplan. “Electrocatalytic reduction of CO2 to formate using particulate Sn electrodes: Effect of metal loading and particle size”. In: *American Journal of Transplantation* 9.6 (2009), pp. 1265–1271. ISSN: 03062619. DOI: 10.1016/j.apenergy.2015.08.012. arXiv: 1112.4730. URL: http://dx.doi.org/10.1016/j.apenergy.2015.08.012.

[32] Sheng Zhang, Peng Kang, and Thomas J. Meyer. “Nanostructured tin catalysts for selective electrochemical reduction of carbon dioxide to formate”. In: *Journal of the American Chemical Society* 136.5 (2014), pp. 1734–1737. ISSN: 00027863. DOI: 10.1021/ja4113885. arXiv: arXiv:1408.1149.

[33] Ruud Kortlever et al. “Catalysts and Reaction Pathways for the Electrochemical Reduction of Carbon Dioxide”. In: *Journal of Physical Chemistry Letters* 6.20 (2015), pp. 4073–4082. ISSN: 19487185. DOI: 10.1021/acs.jpclett.5b01559.

[34] K. J. P. Schouten et al. “A new mechanism for the selectivity to C1 and C2 species in the electrochemical reduction of carbon dioxide on copper electrodes”. In: *Chemical Science* 2.10 (2011), p. 1902. ISSN: 2041-6520. DOI: 10.1039/c1sc00277e. URL: http://xlink.rsc.org/?DOI=c1sc00277e.

[35] Dohyung Kim et al. “Synergistic geometric and electronic effects for electrochemical reduction of carbon dioxide using gold–copper bimetallic nanoparticles”. In: *Nature Communications* 5.May (2014), p. 4948. ISSN: 2041-1723. DOI: 10.1038/ncomms5948. arXiv: 9809069v1 [arXiv:gr-qc]. URL: http://www.nature.com/doifinder/10.1038/ncomms5948.

[36] Jingfu He et al. “Electrocatalytic Alloys for CO2 Reduction”. In: *ChemSusChem* 10 (2017), pp. 1–11. ISSN: 18645631. DOI: 10.1002/cssc.201701825. URL: http://doi.wiley.com/10.1002/cssc.201701825.

[37] Masahiro Watanabe. “Design of Alloy Electrocatalysts for CO[sub 2] Reduction”. In: *Journal of The Electrochemical Society* 138.11 (1991), p. 3382. ISSN: 00134651. DOI: 10.1149/1.2085417. URL: http://jes.ecsdl.org/cgi/doi/10.1149/1.2085417.

[38] Cameron L. Bentley, Minkyung Kang, and Patrick R. Unwin. “Nanoscale Surface Structure–Activity in Electrochemistry and Electrocatalysis”. In: *Journal of the American Chemical Society* 141.6 (Nov. 2018), pp. 2179–2193. DOI: 10.1021/jacs.8b09828.

[39] Ezra L. Clark et al. “Influence of Atomic Surface Structure on the Activity of Ag for the Electrochemical Reduction of CO 2 to CO”. In: *ACS Catalysis* 9.5 (2019), pp. 4006–4014. ISSN: 21555435. DOI: 10.1021/acscatal.9b00260.

[40] Tao Cheng et al. “Predicted Structures of the Active Sites Responsible for the Improved Reduction of Carbon Dioxide by Gold Nanoparticles”. In: *Journal of Physical Chemistry Letters* 8.14 (2017), pp. 3317–3320. ISSN: 19487185. DOI: 10.1021/acs.jpclett.7b01335.

[41] Nathan T. Nesbitt et al. “Liquid–Solid Boundaries Dominate Activity of CO2 Reduction on Gas-Diffusion Electrodes”. In: *ACS Catalysis* 10.23 (Nov. 2020), pp. 14093–14106. DOI: 10.1021/acscatal.0c03319.

[42] Thomas Burdyny and Wilson A. Smith. “CO 2 reduction on gas-diffusion electrodes and why catalytic performance must be assessed at commercially-relevant conditions”. In: *Energy & Environmental Science* 12 (2019), pp. 1442–1453. ISSN: 1754-5692. DOI: 10.1039/c8ee03134g.

2

Role of Potassium Cations During Electrochemical CO_2 Reduction

The specific identity of electrolyte cations has many implications in various electrochemical reactions. However, the exact mechanism by which cations affect electrochemical reactions is not agreed upon in literature. In this report, we investigate the role of cations during the electrochemical reduction of CO_2 by chelating the cations with cryptands, to change the interaction of the cations with the components of the electric double layer. As previously reported we do see the apparent suppression of CO_2 reduction in the absence of cations. However, using in situ- SEIRAS we see that CO_2 reduction does indeed take place albeit at very reduced scales. We also observe that cations play a role in tuning the absorption strengths of not only CO_2 as has been speculated, but also that of reaction products such as CO.[1]

[1] This chapter is in the process of publication

2.1. INTRODUCTION

Electrochemical processes involve charge transfer at the electrode-electrolyte interface which aid chemical reactions such as water splitting and CO_2 reduction (ECO_2R). These interfaces play a crucial role in determining the activity and selectivity of the electrochemical reactions. Changes to the electrode composition, electrode morphology, electrolyte composition, cell architecture, etc., all lead to changes in the electrode-electrolyte interface, thus affecting the reactions.

The identity of the cations used in the electrolyte during electrochemical CO_2 reduction has been shown to affect most electrochemical reactions.[1][2][3][4][5][6] Specifically, as the ionic size of the alkali cation increases, previous works have shown that ECO_2R selectivity at the cathode increases towards CO (on Au and Ag)[1] and towards C2 products (on Cu).[4][5][6] In these cases, it was reported that cations with the largest ionic radius (Cs^+) provided the greatest activity for ECO_2R while the smallest (Li^+) provided the least enhancement. Cations accumulate at the electric double layer (EDL), due to the negatively charged cathode, with concentrations reported to be as much as 80 times the bulk concentrations (at bulk concentrations 0.05M).[7][8][9][10] This condensed layer of cations at the cathode surface is important to understanding mechanisms for ECO_2R, and thus must be included in fundamental understanding and optimization of this reaction.

Many hypotheses have been put forth to describe the role of cations during ECO_2R, however a consensus still has to be reached on how cations and their hydration shells can alter the reactions taking place in the EDL. Specifically adsorbed cations are thought to have stabilizing effects on $*CO_2$ and *COOH- , enabling further protonation and electrochemical reduction.[4][11][12] Cations can also change the concentration profiles of CO_2 at the electrode-electrolyte interface, and can also displace reaction intermediates to more stable reaction sites.[13][14][15] Another theory suggests that the cations directly affect the surface charge density and hence the interfacial electric field thus tuning the adsorption strength of reaction intermediates and also driving the concentration of CO_2 at the interface. [5][16] The key take away from these theories is that the interaction of the cations with the molecular components of the electric double layer (EDL) has a profound effect on the reaction mechanisms and thus activity and selectivity of ECO_2R.

In order to understand the exact nature of the cation's role in electrochemical processes, researchers have used chelating compounds such as crown ethers to change the interaction of the cations with the components of the EDL. [17][18] Crown ethers are 2D cyclic compounds that bind selectively to cations. Their high selectivity for cations is due to the size of their cavity matching the ionic size of the cation. However, another class of compounds called cryptands form much more stable complexes with cations compared to crown ethers. Cryptands are bi or poly-cyclic ethers that also selectively bind to cations. Their higher stability compared to crown ethers is due to their 3D structure that provides a more rigid structure caging in the cation, called a cryptate (Figure 2.1). The complexation rate of these cryptands with the cation in an aqueous solution, compared to the rate of dissociation is much higher ($\sim 10^6$ times), indicating that in a solution with cations and cryptands, at any given moment the cryptate is the dominant component.[19]

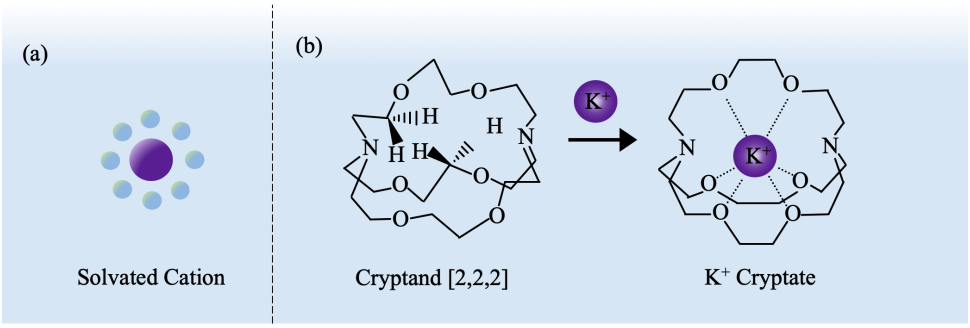

Figure 2.1: *Schematic representation of a potassium cation chelating with Cryptand [2,2,2] to form a K^+ Cryptate.*

2.2. RESULTS AND DISCUSSION

In this report, we elucidate the role of cations in ECO_2R by changing how they interact with the reaction environment by chelating them with cryptands. The cryptands used in this report (Kryptofix [2,2,2]) bind to K^+ ions with very high selectivity and stability due to a match in the ionic size of the K^+ ion and the size of the cavity of the cryptand. [19][20] We study the effect of slowly chelating the cations in the electrolyte with cryptands, during CO_2 reduction over an Ag catalyst in an aqueous H-Cell, where we observed that cations seem to be very crucial for ECO_2R to take place. Using in situ-surface enhanced infrared spectroscopy (SEIRAS) we find that cations directly aid in stabilizing CO_2 onto the surface of the catalyst. We also find that cations may have important interactions with other reaction intermediates and products.

To first understand the effects of chelating K^+ with cryptands, the electrochemical performance of Ag was tested by applying a constant potential in the range of -1.4 to -1.9 V (vs Ag/AgCl) in an aqueous H-cell configuration (complete description of the experiments can be found in the Experimental Section). The performance (current density and Faradaic efficiency) of the Ag catalyst was measured with increasing concentrations of the cryptand to determine its role in driving the reaction activity and selectivity. To understand the baseline activity, the electrochemical performance of Ag was tested in a 0.1M $KHCO_3$ electrolyte. The selectivity for CO gradually increases in this potential range, with the hydrogen evolution reaction (HER) concomitantly being suppressed (Figure 2.2a). With an electrolyte of 0.05M cryptands in 0.1M $KHCO_3$, where a 2:1 ratio of K^+ to cryptands was achieved, the faradaic efficiency (FE) of CO decreased to <10% at all applied potentials (Figure 2.2b). This sudden and large suppression of ECO_2R could indicate that the cryptates move preferentially to the catalyst surface. Chelating all the cations by using an electrolyte with the ratio of K^+ to cryptands being 1:1, completely suppressed the formation of CO, while HER continued (Figure 2.2c). A similar phenomenon where this complete suppression of ECO_2R in the absence of cations have been previously reported.[15][21]

Analyzing the partial current density of CO (jCO) with no cryptands in the electrolyte, gradually increased while the partial current density of hydrogen (jH_2) remained con-

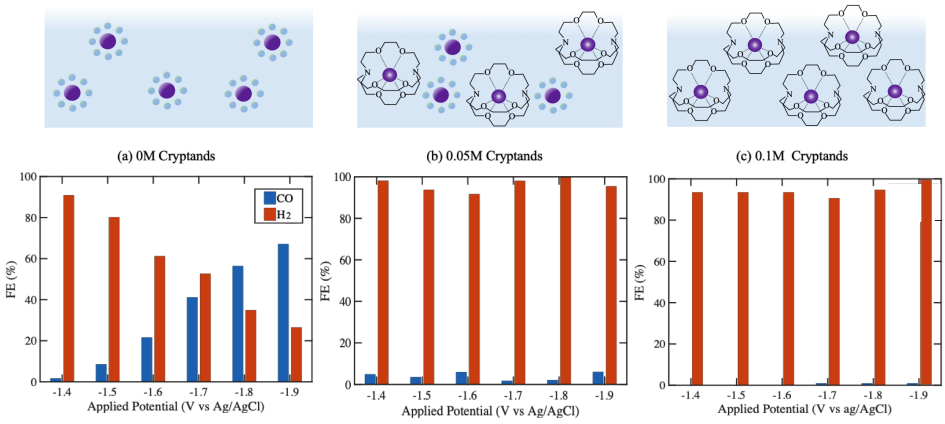

Figure 2.2: *Faradaic Efficiencies recorded in the H-Cell on an Ag catalyst deposited on Ti foil with 0.1M $KHCO_3$ as the electrolyte, (a) with no cryptands, (b) with 0.05M cryptands, (c) with 0.1M cryptands.*

stant. When cryptands were introduced into the electrolyte and their concentration gradually increased, it was observed that the jCO reduces to 0, while the jH_2 almost doubles at all potentials (Appendix A, Figure A.1).

In order to understand the mechanism behind ECO_2R suppression and HER promotion in the presence of cryptands, SEIRAS experiments were conducted to observe the effect of the cryptates on the reaction intermediates at the catalyst surface. A cell specially designed to probe the reaction intermediates was used with Ag deposited onto a Ge crystal.[22] Experiments were conducted with a 0.1M $KHCO_3$ electrolyte, and the cryptands concentration was slowly increased to 0.2M (1:2, K^+:cryptand) by injecting a concentrated cryptand solution into the cell after each experiment (more details of the experiments are provided in Experimental Section). The SEIRAS spectra obtained on an activated Ag catalyst showed multiple distinct vibrational modes. Positive peaks indicate an increase in the concentration of the species whereas negative peaks indicate the depletion of certain species compared to their concentrations during the background scan. The area of these peaks give quantitative information about the species and the position of the peak center provides information on the interaction between the molecule and the catalyst surface.

The CO_2 vibrational mode was observed at ~2340 cm^{-1} as has been previously reported.[22] The peak area of CO_2 however reduces with the increasing concentration of cryptands, indicating a reduced consumption of CO_2 for ECO_2R. However, CO_2 is consumed at all concentrations of cryptands indicating that ECO_2R has surprisingly not been completely suppressed as indicated by the H-cell experiments.

Cations have been proposed to stabilize the adsorbed CO_2 molecule on to the catalyst surface enabling its conversion to various products.[12][14][16] The reduction in CO_2 peak area with increasing cryptand concentrations, suggests that lower quantities of CO_2 is being reduced to CO. This reduction in CO_2 consumption with increasing cryptand concentration, could strengthen the theory of cations stabilizing the $^*CO_2$ molecule on

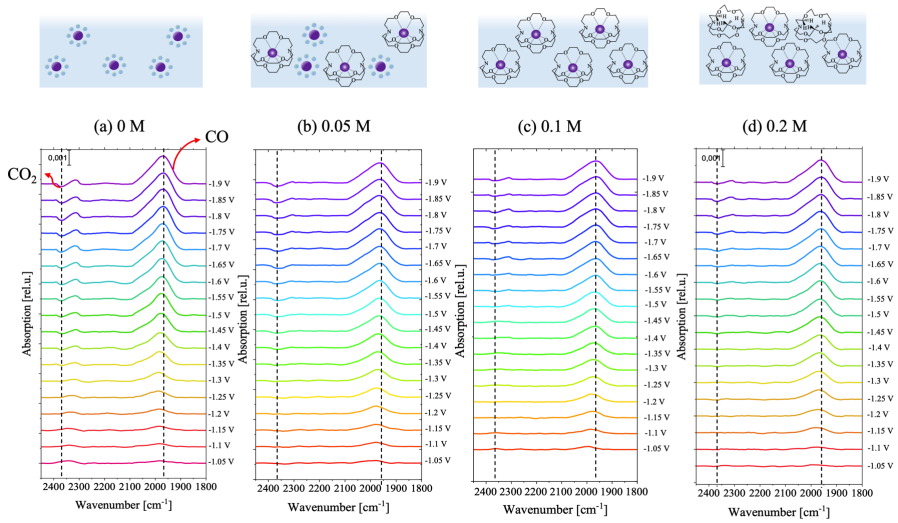

Figure 2.3: *In situ infrared spectroscopy of the electrode surface with different cryptand concentrations, showing the forward scans obtained through applied potentials -1.0V to -1.9V, revealing the peaks for CO_2 and CO with increasing concentrations of cryptands.*

to the catalyst. The forward scans (Figure 2.3) also show that the presence of the CO_2 peak appears at more negative potentials as the cryptand concentration increases, helping to emphasize that cations do help in stabilizing CO_2 on the catalyst surface. However, the mechanism of this stabilizing effect cannot be observed in SEIRAS.

A peak corresponding to the vibrational mode of CO observed in the range of 1990-1970 cm-1 for the baseline experiment without cryptands, which is similar to previously reported values (Figure 2.3).[22][23] As the concentration of cryptands was increased, the CO peaks did not completely vanish from the spectra, as would be expected from the H-Cell results (Figure 2.3). On the contrary, CO peaks were observed at all concentrations of cryptands. There is a stark difference between the CO peak area in the scans with and without cryptands (Figure 2.4a) where increasing concentration of the cryptands had no noticeable effect on the area of the peak. The CO peak areas also only diverge at potentials more negative than -1.4V vs Ag/AgCl, which is the potential at which CO is detected in the H-Cell experiments (Figure 2.4a). The lower peak areas observed with cryptands in the electrolyte could be the result of lower concentrations of CO_2 consumed in the EDL.

The peak centers of CO shifted to lower wavenumbers at more negative potentials. This phenomena has been previously observed and can be attributed to multiple phenomena such as the increased coverage of CO molecules leading more dipole-dipole interactions and well as the Stark tuning effect.[16][22][23][24][25][26]

What was more evident was the shift in the peak centers of CO to lower wavenumbers (~ 15 cm^{-1} at -1.9V vs Ag/AgCl) as the cryptand concentration increased (Figure 2.4b and c). With higher concentrations of cryptands the surface charge density induced by

the cations is lowered and there exists a lower shielding of the negatively charged metal. Therefore, the metal is better equipped to support the adsorbed CO through a more effective pi- backbonding. This causes an increase in bonding strength between the catalyst and the adsorbed CO, which in turn decreases the bond length. The implications of this would lead to an increase in the bond length between the carbon and oxygen atom causing the peak centers of CO to shift to lower wavenumbers. This suggests that the CO molecule is more strongly bound to the metal substrate in the absence of solvated K^+ cations (or by encapsulating the cations in cryptands preventing the cations from directly interacting with the reaction intermediates and products).

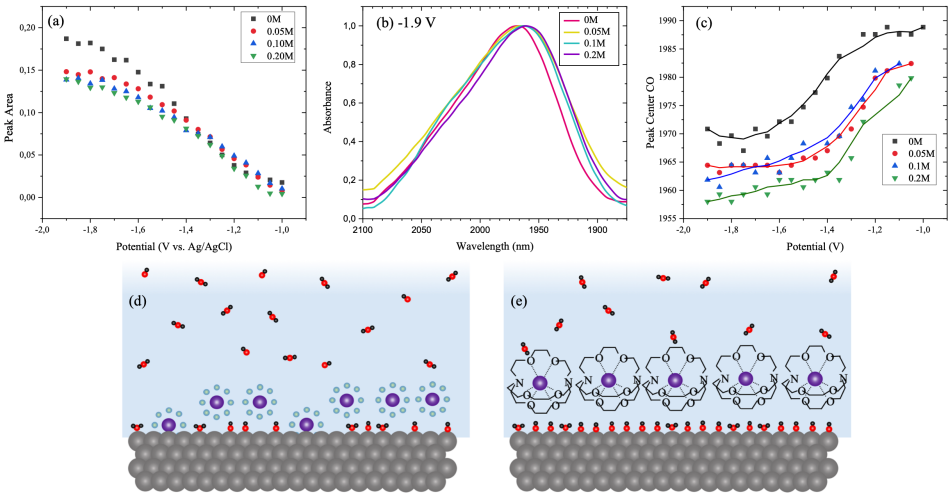

Figure 2.4: *Analysis of CO peak (a) CO peak areas changing with potential (b) Shift in CO peak at -1.9V at different cryptand concentrations (c) Change in CO peak centers with potential at constant cryptand concentration (d) and (e) Schematic representation of cations and cryptates near the catalyst surface.*

To further understand the observed spectroelectrochemical trends, the difference in areas of the CO peaks with and without the cryptands was compared, finding a distinct but narrow change. In the H-cell experiments conducted using electrolytes without cryptands, CO was clearly detected with the GC. The small difference in the peak areas which indicate a small difference in the CO concentrations, implies that CO should have been detected at all concentrations of cryptands. These results thus indicate that the CO molecules remain adsorbed onto the catalyst surface in the absence of K^+ cations.

To confirm the strong adsorption of CO adsorption on the surface, the CO peak areas were monitored during the reverse (going from more negative applied potentials to less negative applied potentials) scans in the SEIRAS (Appendix A, Figure A.2). These data showed that there is no discernable difference in the onset of the reduction in peak area. It was also not possible to cycle at positive potentials in order to observe CO oxidation peaks, as this would damage the catalyst layer on the Ge crystal.[22]

Furthermore, we observed a very small consumption of CO_2 (Figure 2.3) in electrolytes with cryptands, but a constant increase in the peak area of CO which is dispro-

portional to the consumption of CO_2. This could further strengthen the theory that CO concentration is increasing due to it being adsorbed on the catalyst surface and without desorbing.

In summary, we studied the effects of chelating electrolyte cations with cryptands to gain further understanding of the role of cations during the electrochemical conversion of CO_2. We report that by reducing the free cation concentrations in the electrolyte, ECO_2R appears to shut down. Using SEIRAS, we see that the absence of cations does not in fact inhibit ECO_2R, but the lower surface charge density caused the reaction products such as CO to strongly bind to the catalyst surface restricting its desorption. This lowered surface charge density also is seen to lower CO_2 consumption which can be expected from previous literature.

2.3. EXPERIMENTAL METHODS

2.3.1. THIN FILM CATHODE PREPARATION

Thin-film cathodes were deposited on 60º Ge ATR crystals (Pike Technologies, 013-3132). These crystals were polished using alumina powder suspensions of decreasing grain-size (1.0μm, 0.3μm and 0.05μm) and then sonicated for 5 minutes in iso-propyl alcohol and deionized water. Before mounting in the DC magnetron sputtering setup, crystals were wiped with acetone using cotton swabs. Deposition of the Ag catalyst layer was performed in a magnetron sputtering system (PEVAC Project 229), at a chamber pressure of 25µbar, argon flowrate of 15sccm and power rate of 25W, for a deposition rate between 0.013 and 0.014nm/s and thickness of 40nm. Presence of the catalyst was confirmed both optically and by measuring the resistance over the film using a multimeter, which was between 3 and 4ω. This procedure is strongly based to one reported in previous literature, but avoids air- or argon-plasma cleaning of the target while delivering comparable results.[22][27]

2.3.2. ELECTROCHEMICAL SEIRAS ROUTINES

Electrochemical SEIRAS measurements were performed in a proprietary H-cell which accommodates the crystal as working electrode. A graphite rod (Alfa Aesar, 99.9995% metals basis) served as the counter electrode, whilst the reference was a 3M NaCl Ag/AgCl miniaturized electrode (BASI, MF-2052). The electrolyte used was 0.1M $KHCO_3$ (Sigma-Aldrich, 99.7% ACS reagent), to which a 0.5M cryptand (Kryptofix [222] Sigma Aldrich 99%) solution was added to achieve the target concentration. SEIRAS spectra were collected in a Brucker Vertex 70 modified FT-IR spectrometer, averaged over 72 scans at a resolution of 4cm-1. These spectra were collected as reflectance of the signal and transformed to absorbance units (a.u.) using the relation: A = -log(R/R0 The sample chamber accommodates the proprietary cell and an additional N2 purge (see Fig.S2). Electrochemical routines were performed using a BioLogic SP-200 potentiostat. Before any spectroscopic measurement, the cell was purged for 30 min. using 99.999% pure CO_2 gas (5 sccm). This purge was also active during electrochemistry. Before starting SEIRAS experiments, the Ag thin film was activated by applying 6 cyclic voltammetries from +0.2V to -1.1V vs. Ag/AgCl. After this, background scans were collected at -0.5V vs. Ag/AgCl, and consecutive scans every 50mV during a linear sweep voltammetry at 2mV/s. At -1.9V,

the potential was held for 7 scans before being reversed to OCV at the same scan-rate.

2.3.3. ELECTROCHEMICAL MEASUREMENTS

The electrochemical reduction of CO_2 was conducted in a homemade custom H-cell. The cell's body was made of Polymethyl methacrylate (PMMA) with Pt as the anode and a cation exchange membrane (Nafion NM 115 from Ion Power), separating the anode chamber from the cathode chamber. A CO_2 purge stream was constantly fed to both the anolyte and catholyte at 10 sccm each. The electrolyte used was 0.1 M $KHCO_3$ saturated with CO_2. Electrolytes with Cryptands (Kryptofix[222] Sigma Aldrich 99%) were prepared in 0.1M $KHCO_3$ solutions and fresh electrolytes were used after every experiment. The reference electrode used was Ag/AgCl and the catholyte was constantly stirred with a magnetic stirrer to improve mass transport. Experiments were conducted by applying a constant potential (-1.4 V to -1.9 V) and measuring the current over the span of 60 minutes. The overhead gas space of the catholyte was sampled every 10 minutes by an online Gas Chromatograph (GC) (Compact GC 4.0, GAS) to determine the gaseous products formed.

BIBLIOGRAPHY

[1] Michael R. Thorson, Karl I. Siil, and Paul J.A. Kenis. "Effect of cations on the electrochemical conversion of CO2 to CO". In: *Journal of the Electrochemical Society* 160.1 (2013). ISSN: 00134651. DOI: 10.1149/2.052301jes.

[2] Charuni M. Gunathunge, Vincent J. Ovalle, and Matthias M. Waegele. "Probing promoting effects of alkali cations on the reduction of CO at the aqueous electrolyte/copper interface". In: *Physical Chemistry Chemical Physics* 19.44 (2017), pp. 30166–30172. ISSN: 14639076. DOI: 10.1039/c7cp06087d.

[3] Onagie Ayemoba and Angel Cuesta. "Spectroscopic Evidence of Size-Dependent Buffering of Interfacial pH by Cation Hydrolysis during CO2 Electroreduction". In: *ACS Applied Materials and Interfaces* 9.33 (2017), pp. 27377–27382. ISSN: 19448252. DOI: 10.1021/acsami.7b07351.

[4] Akira Murata and Yoshio Hori. *Product selectivity affected by cationic species in electrochemical reduction of CO2 and CO at a Cu electrode*. 1991. DOI: 10.1246/bcsj.64.123.

[5] Joaquin Resasco et al. "Promoter Effects of Alkali Metal Cations on the Electrochemical Reduction of Carbon Dioxide". In: *Journal of the American Chemical Society* 139.32 (2017). ISSN: 15205126. DOI: 10.1021/jacs.7b06765.

[6] Meenesh R. Singh et al. "Hydrolysis of Electrolyte Cations Enhances the Electrochemical Reduction of CO2 over Ag and Cu". In: *Journal of the American Chemical Society* 138.39 (2016), pp. 13006–13012. ISSN: 15205126. DOI: 10.1021/jacs.6b07612.

[7] Stephen E. Weitzner et al. "Toward Engineering of Solution Microenvironments for the CO2Reduction Reaction: Unraveling pH and Voltage Effects from a Combined Density-Functional-Continuum Theory". In: *Journal of Physical Chemistry Letters* 11.10 (2020), pp. 4113–4118. ISSN: 19487185. DOI: 10.1021/acs.jpclett.0c00957.

[8] Divya Bohra et al. "Modeling the electrical double layer to understand the reaction environment in a CO2 electrocatalytic system". In: *Energy and Environmental Science* 12.11 (2019), pp. 3380–3389. ISSN: 17545706. DOI: 10.1039/c9ee02485a.

[9] Batyr Garlyyev et al. "Influence of the Nature of the Alkali Metal Cations on the Electrical Double-Layer Capacitance of Model Pt(111) and Au(111) Electrodes". In: *Journal of Physical Chemistry Letters* 9.8 (2018), pp. 1927–1930. ISSN: 19487185. DOI: 10.1021/acs.jpclett.8b00610.

[10] Jianan Erick Huang et al. "CO 2 electrolysis to multi-carbon products in strong acid". In: *Science* 372 (2021), pp. 1074–1078.

[11] B Damaskin. “Weak specific adsorption of ions”. In: *Journal of Electroanalytical Chemistry* 65.2 (Oct. 1975), pp. 799–814. DOI: 10.1016/0368-1874(75)85159-8. URL: https://doi.org/10.1016/0368-1874(75)85159-8.

[12] Irina V. Chernyshova and Sathish Ponnurangam. “Activation of CO 2 at the electrode-electrolyte interface by a co-adsorbed cation and an electric field”. In: *Physical Chemistry Chemical Physics* 21.17 (2019), pp. 8797–8807. ISSN: 14639076. DOI: 10.1039/c8cp07807f.

[13] M. Dunwell et al. “Surface enhanced spectroscopic investigations of adsorption of cations on electrochemical interfaces”. In: *Physical Chemistry Chemical Physics* 19.2 (2017), pp. 971–975. ISSN: 14639076. DOI: 10.1039/c6cp07207k.

[14] Leanne Chen et al. “Electric Field Effects in Electrochemical CO 2 Reduction”. In: *ACS Catalysis* 6.10 (2016), pp. 7133–7139. ISSN: 2155-5435. DOI: 10.1021/acscatal.6b02299.s001.

[15] Mariana C. O. Monteiro et al. “Absence of CO2 electroreduction on copper, gold and silver electrodes without metal cations in solution”. In: *Nature Catalysis* 4.8 (July 2021), pp. 654–662. DOI: 10.1038/s41929-021-00655-5. URL: https://doi.org/10.1038/s41929-021-00655-5.

[16] Stefan Ringe et al. “Understanding cation effects in electrochemical CO2 reduction”. In: *Energy and Environmental Science* 12.10 (2019), pp. 3001–3014. ISSN: 17545706. DOI: 10.1039/c9ee01341e.

[17] Arthur G. Fink et al. “ Impact of Alkali Cation Identity on the Conversion of HCO 3 - to CO in Bicarbonate Electrolyzers ”. In: *ChemElectroChem* 8.11 (2021), pp. 2094–2100. ISSN: 2196-0216. DOI: 10.1002/celc.202100408.

[18] A. S. Malkani et al. “Understanding the electric and nonelectric field components of the cation effect on the electrochemical CO reduction reaction”. In: *Science Advances* 6.45 (2020). ISSN: 23752548. DOI: 10.1126/SCIADV.ABD2569.

[19] George W Gokel. *Chapter 3. Complexation by Crowns and Cryptands*. 2016, pp. 64–98. ISBN: 9781788010917. DOI: 10.1039/9781788010917-00064.

[20] G Wipff and P Auffinger. “Hydration of the 222 Cryptand and 22 Cryptates Studied by Molecular Dynamics Simulations”. In: *Journal of the American Chemical Society* 113.14 (1991), pp. 5976–5988.

[21] A. N. Frumkin. “Influence of cation adsorption on the kinetics of electrode processes”. In: *Transactions of the Faraday Society* 55.1 (1959), pp. 156–167. ISSN: 00147672. DOI: 10.1039/tf9595500156.

[22] Elizabeth R. Corson et al. “In Situ ATR-SEIRAS of Carbon Dioxide Reduction at a Plasmonic Silver Cathode”. In: *Journal of the American Chemical Society* 142.27 (2020), pp. 11750–11762. ISSN: 15205126. DOI: 10.1021/jacs.0c01953.

[23] Sohail Anjum Shahzad. “Carbon Monoxide Adsorption on Copper and Silver Electrodes during Carbon Dioxide Electroreduction Studied by Infrared Reflection Absorption Spectroscopy and Surface-Enhanced Raman Spectroscopy”. In: *Langmuir* 12.4 (1996), pp. 1094–1097. DOI: 10.1007/978-3-642-33173-2_5.

[24] Matthias M. Waegele et al. “How cations affect the electric double layer and the rates and selectivity of electrocatalytic processes”. In: *Journal of Chemical Physics* 151.16 (2019). ISSN: 00219606. DOI: 10.1063/1.5124878. URL: https://doi.org/10.1063/1.5124878.

[25] David K. Lambert. “Vibrational Stark effect of CO on Ni(100), and CO in the aqueous double layer: Experiment, theory, and models”. In: *The Journal of Chemical Physics* 89.6 (1988), pp. 3847–3860. ISSN: 00219606. DOI: 10.1063/1.454860.

[26] A. Görling et al. “On the coadsorption of CO and alkali atoms at transition metal surfaces: A LCGTO-LDF cluster study”. In: *Surface Science* 286.1-2 (1993), pp. 26–45. ISSN: 00396028. DOI: 10.1016/0039-6028(93)90553-V.

[27] Nienke J. Firet and Wilson A. Smith. “Probing the Reaction Mechanism of CO2 Electroreduction over Ag Films via Operando Infrared Spectroscopy”. In: *ACS Catalysis* 7.1 (Dec. 2016), pp. 606–612. DOI: 10.1021/acscatal.6b02382.

3

AuSn Intermetallic System for CO_2 Reduction in H-Cell

Carbon dioxide can be electrochemically converted into feedstocks for many industrial processes such as the manufacturing of synthetic fuels and chemicals. This work focuses on the structure-functionality relationship between Au, Sn, and bimetallic AuSn catalysts, and their CO_2 reduction performance in an H-Cell at varying current densities. X-Ray diffraction (XRD), X-ray photoemission spectroscopy (XPS), and atomic force microscopy (AFM) were used to determine the crystal structure, surface morphology and composition of compositionally variant bimetallic thin films of Au-Sn before and after electrolysis. The electrochemical activity for each bimetallic film was measured in terms of electrode current and product selectivity as a function of applied current density and catalyst composition. The results of this work show that not all combinations of metals for CO_2 reduction can improve catalyst activity towards a desired product. And that a detailed material characterization can help in drawing structure-functionality relationships between a catalyst and its activity.

3.1. Introduction

Considering the present climate scenario, there is an urgency to drastically reduce CO_2 emissions into the atmosphere, requiring policy makers and researchers around the globe to look for solutions to slow down the effects of global climate change. This challenge has sparked various scientific research programs including CO_2 capture[1], biological transformation of CO_2 using microbes[2], thermal conversion of CO_2[3], and electrochemical conversion of CO_2.[4] The latter approach provides a method to use electricity generated from renewable sources to convert CO_2 into a multitude of value of added products. The decreasing cost of solar and wind produced electricity can help drive down the cost of electrochemically derived chemicals[5] and fuels, which can potentially enable a transition on the global energy landscape. The electrochemical conversion of CO_2 is capable of reducing CO_2 into products such as CO, formate, ethylene, and various other hydrocarbons, whose selectivity is strongly influenced by the catalyst used.[6][7][8] Au, Ag and Zn have shown high selectivity to CO[9][10][4], Sn and Pb selectively produce formate[11][12], while Cu can produce a wide array of C+ and C_2+ products.[13][10] In order for the electrochemical reduction of CO_2 to gain industrial relevance in producing value added products, a series of fundamental and applied challenges must be overcome to improve performance metrics of the conversion process.[8] CO_2 molecules are stable and have low solubility (1.5 g per 1000 g water) in water, which leads to slow kinetics of CO_2 reduction reactions resulting in low current densities and poor selectivities compared to the hydrogen evolution reaction (HER). To increase the solubility and decrease the diffusion length of CO_2, several approaches have been taken including using 5 catalysts with high surface areas[14], electrolytes that have a higher affinity to CO_2[15], gas diffusion electrode (GDE)[11], or operation at high pressure.[16][17] Other approaches include altering the electronic structure of catalyst surfaces by making alloy or bimetallic thin films and nanoparticles to tune the binding energy of one of more reaction intermediates.

Traditionally, most studies focus on the characterization of pure metal catalysts.[9][13][18][19] However, it has been shown that alloying different metals can have an advantageous effect on the selectivity and activity of the catalyst for CO_2 reduction.[20][21][22][23][24]For example, there have been a number of studies that showed that the selectivity for CO on gold was increased by alloying it with Cu.[13][25]By controlling the composition of catalysts, it is possible to alter the electronic structure of the catalyst surface, which allows the ability to steer product selectivity. However, many studies that have examined the selectivity and activity changes in alloy and bimetallic catalysts have examined nanostructured materials, which can produce both electronic and morphological changes that affect the reaction mechanism. The ability to separate morphological and electronic effects to tune product selectivity is critical to provide mechanistic information about what drives product selectivity in bimetallic and alloyed CO_2 reduction catalysts. Here, we investigate the ability to tune the selectivity of CO_2 reduction by alloying different metals in a thin film architecture, and examining their electrochemical performance as a function of applied potential and current density. As Au is one of the most widely studied catalysts for its high CO selectivity[9][6],we studied the effects of mixing Au with Sn, which in turn is known for its high formate selectivity and its ability to suppress the

production of hydrogen, the latter of which is the only competing undesirable reaction on Au.[26][27] thin films of Au, Sn, and three bimetallic compositions of AuSn were deposited by RF magnetron sputtering onto Ti substrates, and their morphological, electronic, and electrocatalytic properties were evaluated under identical conditions. Thin films were chosen as a platform for this study to attempt to investigate electronic and compositional changes in AuSn catalysts without having significant morphological influences from nanostructuring, which may alter the reaction mechanism by changing the local environment due to mass transport effects. The results of this study show that the activity and selectivity of the CO_2 reduction reaction was influenced by both the electronic structure and composition of the thin films, and that the addition of Sn to Au does not improve the selectivity towards CO like other metals have shown previously.

3.2. EXPERIMENTAL SECTION

RF magnetron co-sputtering was used to deposit thin films of various Sn and Au compositions onto Ti (0.25mm thick foil, 99.5%, Alfa Aesar) substrates based on the method published previously.[20] The composition of the thin films was controlled by varying the DC power supplied to the pure Au (99.99%, MaTeck GmbH) and Sn (99.99%, MaTeck GmbH) metal targets, and the thickness was controlled by the duration of the sputtering (200 nm) and checked by a quartz crystal microbalance (QCM). The different powers supplied and the expected compositions are detailed in the Appendix B (Table B.1).

X-Ray Diffraction (XRD) patterns (10°–90°2θ) for the as prepared samples were collected by a Bruker D8 Advance X-ray diffractometer using a cobalt source (λ = 1.7889 Å) in Bragg–Brentano configuration. After electrolysis, samples were removed from the electrochemical cell inside a nitrogen filled glove box and were analyzed in an air-tight XRD sample holder to reduce the effects of atmospheric oxidation that may occur when transferring the sample from the electrochemical cell to the XRD.

X-Ray Photoelectron Spectroscopy (XPS) experiments were conducted using a Thermo Scientific K- alpha apparatus equipped with an Al K-alpha X-ray Source and a flood gun to avoid charging of the sample. Parameters used for the measurements were: spot size of 400 μm, pass energy of 50 eV, energy step size of 0.1 eV, dwell time of 50 ms,and 10 scans in the vicinity of Au 4f, Sn3d, O1s and C1s orbital binding energies. To obtain valence band spectra, the number of scans was increased to 100. XPS spectra were corrected using the 1s peak from atmospheric carbon (284.8 eV).

Surface morphologies were mapped using a Bruker Dimension Icon atomic force microscope (AFM) using a TESPA-V2 cantilever in tapping mode.

The electrochemical reduction of CO_2 was conducted in a homemade custom H-cell. The cell's body was made of Polymethyl methacrylate (PMMA) with Pt as the anode and a cation exchange membrane (Nafion NM 115 from Ion Power), separating the anode chamber from the cathode chamber. A CO_2 purge stream was constantly fed to both the

anolyte and catholyte at 10 sccm each. The electrolyte used was 0.1 M $KHCO_3$ saturated with CO_2. The reference electrode used was Ag/AgCl and the catholyte was constantly stirred with a magnetic stirrer to improve mass transport. Experiments were conducted by applying a constant current density (1, 5, 10 mA/cm^2) and measuring the potential over the span of 60 minutes. The overhead gas space of the catholyte was sampled every 10 minutes by an online Gas Chromatograph (GC)(Compact GC 4.0, GAS) to determine the gaseous products formed. The catholyte was also sampled every 10 minutes to analyze the liquid products formed over time. Liquid samples were analyzed using an Agilent high performance liquid chromatograph (HPLC) system with an isocratic pump, pumping the mobile phase (0.02 M H_2SO_4) with a part of the liquid samples through a Hi Plex H column. The flow rate of the mobile phase was set at 0.6 ml/min with injection volume being 50 μl. The products were detected using a visible wavelength detector and refractive index detector.

3.3. Results and Discussion

3.3.1. Characterization of The Au/Sn Bimetallic Catalysts

Thin films of Au, Sn, and 3 compositionally variant combinations of Au-Sn were deposited on Ti foil substrates by RF magnetron sputtering. Prior to electrolysis, the films were characterized by AFM, XRD, and XPS to obtain morphological, crystalline and surface electronic/compositional information respectively. Post electrolysis a similar characterization of the samples was conducted.

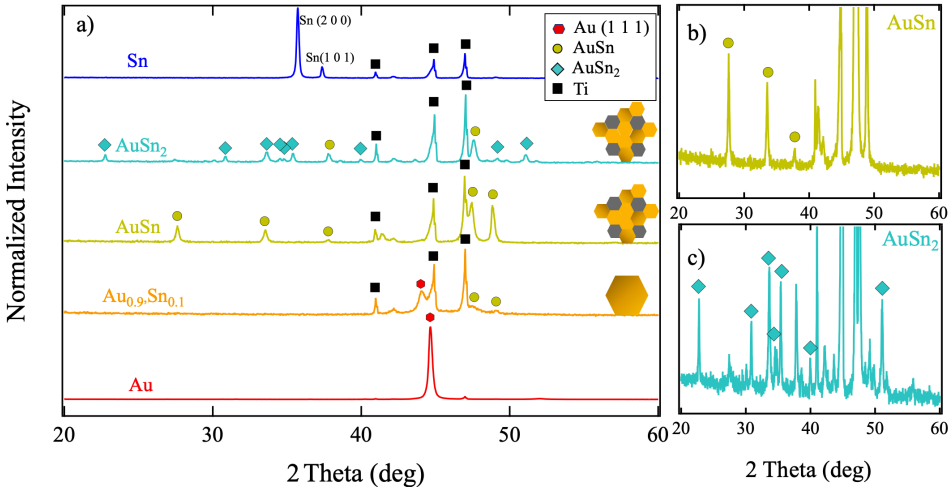

Figure 3.1: *(a) XRD diffractograms of Au, $Au_{0.9}Sn_{0.1}$, AuSn, $AuSn_2$, and Sn thin films. $Au_{0.9}Sn_{0.1}$, AuSn, and $AuSn_2$ are schematically represented alongside their X-ray diffraction patterns. (b, c) Enlarged images of AuSn and $AuSn_2$, respectively.*

The XRD patterns for the 5 thin film compositions are shown in Figure 3.1. The pure metal films show distinct diffraction peaks that are characteristic of the face centered

cubic (FCC) and tetragonal crystal structures for Au and Sn, respectively. From here on out the samples are labelled as follows 1) Au – pure gold, 2) $Au_{0.9}$,$Sn_{0.1}$ (as this is the average bulk composition of the high Sn content sample as detected by using the XPS, detailed later), 3) AuSn, 4)$AuSn_2$ (these are the intermetallic phases detected), 5)Sn – pure tin. The diffractogram of the pure Au thin film shows a preferred orientation along the (111) direction. The addition of a slight amount of Sn was achieved by decreasing the power supplied to the Au target and increasing the power supply to the Sn target in the deposition process (the power supplied to each of the targets and the expected compositions are listed in Table S1). The resulting films showed a shift of the (111) peak of Au to lower diffraction angles (depicted in Figure 3.1). The peak shifts most likely arise from a strained Au lattice due to the introduction of a small amounts of Sn. In addition, small peaks are observed at 2θ = 47.6°and 49°, which are indicative of the AuSn alloy phase. These peaks are very small compared to the Ti substrate and Au (111) peaks, and thus may compromise a very small volume of the 200nm thin films. The small addition of AuSn may explain the shift of the Au (111) peak, which may be due to a strained lattice from the incorporation of small AuSn domains. The initial addition of Sn into Au also may create a solid solution, as the two elements have similar atomic sizes, where Au has an atomic radius of 1.59 Å, and Sn has an atomic radius of 1.63 Å.[28] These radii are less than 15% different, which is generally considered as the upper limit for substitutional doping. Using Braggs law, the lattice constant of the Au film with a small amount of Sn added was calculated to be 4.13 Å. This is indeed greater than the experimental lattice constant of FCC Au (4.08 Å[29]). However, the solubility of Sn into Au has a limit which is defined by the valency of the solute atoms. [28] The higher the valency of the solute atom the smaller its maximum solubility. Sn, on the other hand is tetravalent and its solubility in Au is limited to 6.6% at 532°C.[30]

As the amount of Sn was further increased in the depositions, new peaks in the XRD diffractograms emerged that had characteristics of the AuSn[31] and $AuSn_2$ bimetallic phases.[32] The $AuSn_2$ phase has a NiAs-type hexagonal lattice and is a subtractional solid solution which typically contains Au vacancies.[28] The $AuSn_2$ phase has an orthorhombic crystal structure and shows a very narrow homogeneity range which can be seen by the low intensity reflections and in the phase diagram of the Au/Sn system.[30] the three intermediate compositions are not pure alloys of Au and Sn, as the XRD[33] patterns show. At a low Sn ratio, Sn is initially dissolved into the Au lattice, while as the amount of Sn was increased in the sputtering deposition, two distinct intermetallic phases of AuSn are formed.[33]

XRD diffractograms of the samples collected after electrolysis (Appendix B, Figure B.1) showed that the bimetallic systems maintain their as-synthesized crystal structures after CO_2 reduction.

AFM scans were recorded for each of the five thin-film compositions before electrolysis, shown in Figure 3.2(a to e). The height images were compared to the phase images to enhance the details of the surfaces. Phase images provide information about changing mechanical properties across a surface but do not provide information on which mechanical properties. The Au films look relatively smooth with small (~10 nm) spheres dispersed uniformly over the surface. However, the pure Sn films have large crystallites with well defined facets and edges on their surface. The $Au_{0.9}$,$Sn_{0.1}$ films retain the flat

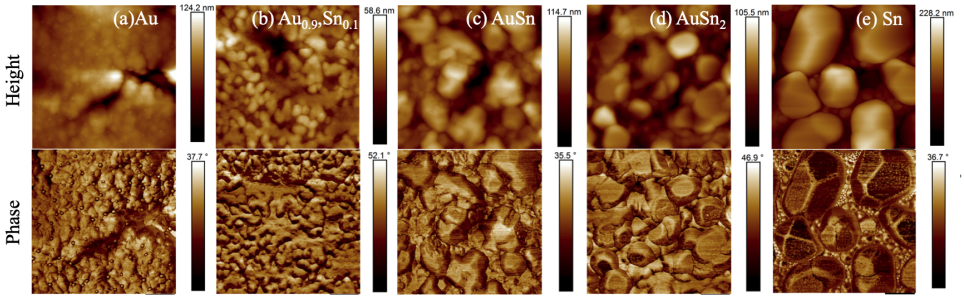

Figure 3.2: *(a-e) AFM images of Au, Au0.9,Sn0.1, AuSn, AuSn2, and Sn thin films, with a scan area of 1 µm × 1 µm. The top row shows the respective height sensor images, and the bottom row shows the phase images of the same scan area.*

surface of Au but become distorted by the addition of Sn. The AuSn and $AuSn_2$ films show the presence of large agglomerates on the surface, which look like distorted Sn crystallites, albeit without the well-defined edges and facets of pure Sn. These images show that the three intermediate compositions of Au and Sn have some resemblance in their morphology to their parent materials. The roughness of these surfaces was also calculated and is shown in the Appendix B (Table B.2). In general, the surfaces are relatively smooth, as is characteristic of sputtered surfaces; however, there is a slight increase in the roughness values of the surfaces with the addition of Sn to Au.

AMF scans of the thin films recorded after electrolysis (Appendix B, Figures B.3 and B.4) show considerable morphological changes. All samples show the appearance of spheres on their surfaces. $Au_{0.9}$,$Sn_{0.1}$ loses its undulating surface, and big (~60 nm) agglomerates appear on its surface, which appear to be different from the rest of the surface. The agglomerates on AuSn and $AuSn_2$ are not as defined as they were before electrolysis but can still be distinguished. Similar results are observed for Sn; the well-faceted surface of Sn is lost, and smaller undefined spheres have appeared.

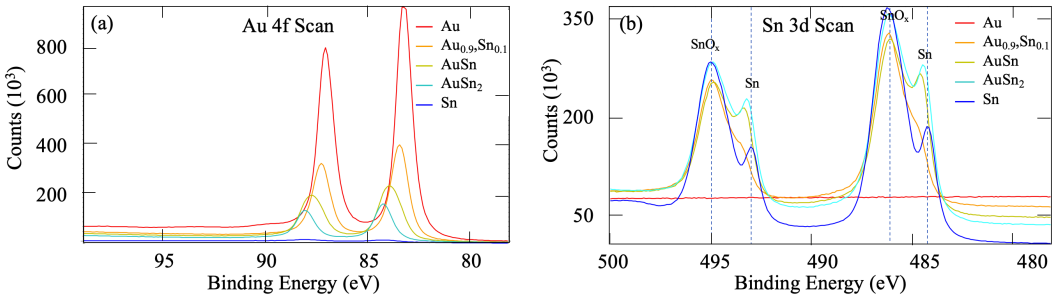

Figure 3.3: *XPS spectra of the Au 4f orbital and Sn 3d orbital, obtained from the different composition thin films*

XPS was also performed on the surface of all five thin films before electrolysis, and the results are grouped by atomic composition, with the XPS spectra of the Au 4f orbital

shown in Figure 3.3a and the Sn 3d orbital in Figure 3.3b. As the amount of Sn was increased in the films, the peaks of the 4f orbitals of Au at 84 and 87.5 eV shifted to higher binding energies and reduced in magnitude, until a flat spectrum was observed for the pure Sn thin film.

A shift in the binding energy of electrons to higher energies can be due to changes in the electrostatic shielding of the nuclear charge from the electrons, or the removal or addition of electrons. The shift in binding energies has also been suggested to correspond to changes in the resistivity of the sample, which could be due to the addition of Sn to Au[34] (Au: 2.34 × 10–8 Ωm; Sn: 1.49 × 10–7 Ωm). However, the shift in binding energy could also be due to the partial withdrawal of electrons from Au atoms due to the addition of Sn, which is more electronegative. The Au peak for the $AuSn_2$ film shows the maximum shift to 85 eV. A peak at this binding energy has been attributed to the $AuSn_4$ phase, although this phase was not found in the previous XRD results.[35] This could be due to XRD being a bulk analysis method, while XPS is a surface analysis technique, meaning that the $AuSn_2$ films may have a surface layer of $AuSn_4$ on top or a surplus of phase-segregated Sn.

For the pure Sn thin films, the peaks detected are more complex due to the presence of $SnO_{(x)}$ peaks so close to the Sn peaks. The 3d orbital scans of Sn depict both the peaks for metallic Sn (485 and 493 eV) and SnO/SnO_2 (487 and 495 eV). With the increasing Sn concentration, there is a slight shift of the Sn peaks from 485.3 to 485 eV, which is not as considerable as the shift observed for Au. The amount of SnO_x gradually increases with the amount of Sn. The presence of SnO_x was not detected in the XRD patterns, suggesting that the SnO_x present is either amorphous or found only as a thin layer on the surface, most likely due to oxidation of the samples when transferring from the sputtering chamber to the XPS vacuum chamber.

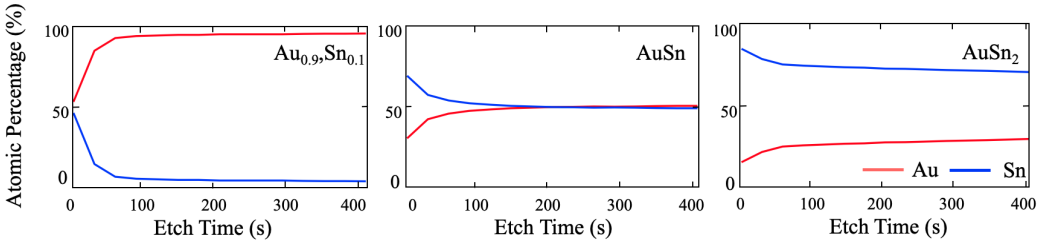

Figure 3.4: *XPS depth profiles for the three bimetallic thin-film compositions.*

XPS depth profiling was also conducted in order to understand the change in the composition/structure (if any) throughout the thickness of the thin films. An argon ion gun in the XPS was used to slowly etch away the surface of the samples for a total of 400 s each, which corresponds to a depth of about ~50 nm. This was estimated by measuring the amount of time that was needed to etch away the entire thin film until Ti was detected, at the same ion gun power. The XPS was used at intervals of 30 s to reveal the composition as a function of thickness. The depth profiles of the three bimetallic films are shown in Figure 3.4, which depict the change in composition from the surface (left hand side of each plot) to the bulk of the sample (right hand side). The intermediate

compositions all show a more Sn-rich surface, with a roughly ~8 nm thickness of enriched Sn. This thickness of a surplus of Sn for the intermediate compositions is likely due to the formation of the native SnO_x layer that forms due to exposure to air, which would thus not show up in the XRD patterns. Therefore, even with different amounts of Au in the bimetallic films, the catalytic activity may be still dominated by Sn, which oxidizes to SnO_x in air, but will reduce to metallic Sn under electrochemically reducing conditions. This effect of surface enriched Sn has been seen in the Au/Sn bimetallic system when it has been used as a solder[36] and as a nanoparticle for CO_2 reduction.[27] However, it is important to note that these measurements were made under high vacuum, and under reducing electrochemical conditions, the surface may re- structure to a different composition (dissolution, phase separation, thermodynamic stability, etc.).

3.3.2. Electrochemical CO_2 Reduction over Bimetallic, Au, and Sn Thin Films.

Once the physical, chemical, and structural properties of the bimetallic films were characterized, the electrochemical performance was assessed using chronopotentiometry at applied current densities of 1, 5, and 10 mA/cm^2. Chronopotentiometry was used since it has been shown recently that the local environment near the catalyst surface changes significantly as a function of current density,[37] and so here, we probe how this can affect product selectivity. In Figure 3.5, the faradaic efficiency (FE) is plotted as a function of the applied current density and composition. The selectivity for CO reaches a maximum at 5 mA/cm^2 with Au (Figure 3.5 a), after which at 10 mA/cm^2, the mass transport limited region of the H-cell is reached, resulting in an increase in the evolution of H_2.[37] When Sn is introduced into Au with a low quantity of $Au_{0.9}$,$Sn_{0.1}$, at low current densities (1 mA/cm^2) the selectivity to CO drops to 0%, but formate is still produced with a FE of ~10% (Figure 3.5b). Increasing the current density increases the selectivity of CO to ~3% and that of formate decreases slightly to ~6%. The FE of H_2 using AuSn is lower than that using the $Au_{0.9}$,$Sn_{0.1}$ film, while that of CO and formate increases to ~8% and ~18%, respectively. Increasing the current density decreases the selectivity for both the CO_2 reduction products. Increasing the composition of Sn further to form $AuSn_2$ suppresses the HER, and the FE of CO and formate increases to ~12% and ~51%, respectively. Pure Sn provides a mixture of CO and H_2 at 1 mA/cm^2, and a formate selectivity of ~34%. At 5 mA/cm^2, the selectivity for formate is at its highest ~67%, while that for CO and H_2 decreases. Increasing the current density suppresses the selectivity toward CO_2 reduction, and once again, H_2 evolution takes over.

To examine how much current went to the formation of each product, the partial current density is plotted in Figure 3.6a–c. At low current densities (Figure 3.6a), the CO partial current abruptly decreases accompanied by a drastic increase in the production of hydrogen upon the inclusion of Sn. At the same time, formate production increases steadily with the addition of Sn. The initial drastic fall in the selectivity for CO with the addition of Sn at all current densities even though the crystal structure of Au is retained is a very interesting phenomenon. Both Au and Sn possess higher selectivities for CO upon CO_2 reduction, as can be seen from Figure 3.5. However, changes induced to the

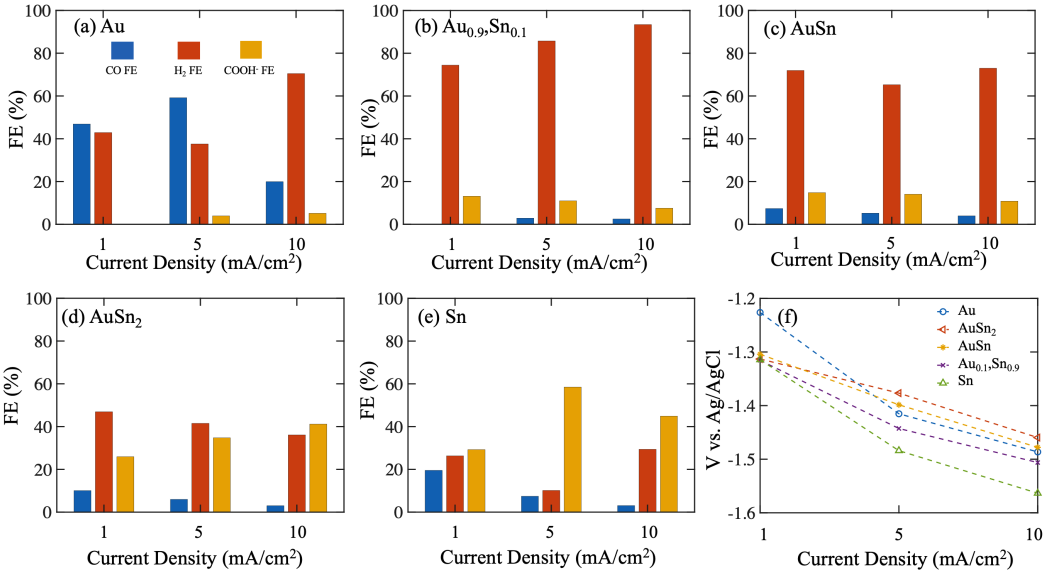

Figure 3.5: *((a-e) Change in faradaic efficiency (FE) and measured potential with composition and current density. The FE depicted is the averaged FE over the entire 60 min of each experiment after stabilization. (f) Potentials depicted have been corrected for ohmic drop. show*

Au lattice and binding energies upon the addition of Sn alter this selectivity and reduce the systems' activity for CO_2 reduction. Increasing the Sn percentage, increases the selectivity for CO marginally and that of formate considerably. The addition of Sn also suppresses the HER, compared to increased partial current density for CO_2 reduction products.

Influence of the Gold Valence Band on CO Production. From the previously discussed characterization, the only two factors changing between Au and the $Au_{0.9}$,$Sn_{0.1}$ films are the bulk lattice constants and the increasing binding energy of Au by the addition of Sn. In order to understand the trend over all the compositionally variant catalysts, the valence band structures were also obtained via XPS, and the valence band structures of Au and the bimetallic films are plotted in Figure 3.7. Here, the intensities of the valence band structures have been normalized, and the averaged d-band centers of the valence bands are shown as colored bars at the bottom of the graph (see the calculation of the d-band center in Appendix B. Figure B.2).

The valence d-band structures of only Au are indicated here, since the valence structures seen here are mainly due to the contributions of Au d-orbitals.[38] Sn does not possess any valence d-orbitals, and the contribution of the valence Sn p-orbital to the valence band structures is very low, compared to that of Au (un-normalized valence band structures of all the different compositions can be seen in Appendix B, Figure B.2). Hence, its overall contribution to the shape of the valence bands of the bimetallic sys-

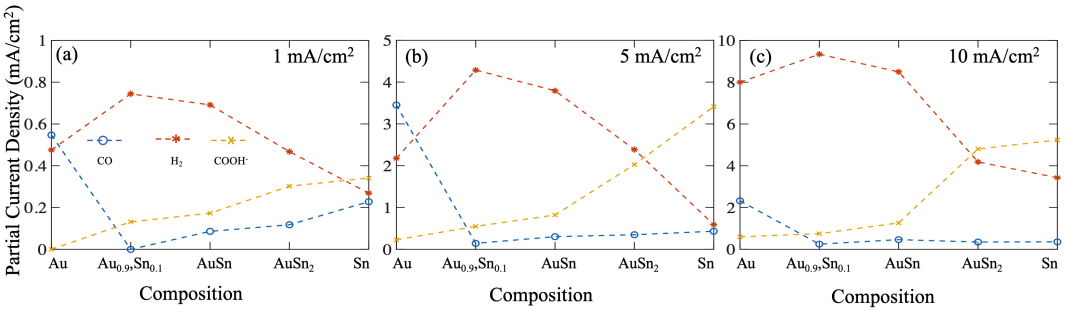

Figure 3.6: *Change in partial current density with composition at constant current density.*

tems is negligible. The higher the energy of the d-band center with respect to the fermi energy level, the higher the energy of the antibonding states and stronger the bond.[39]

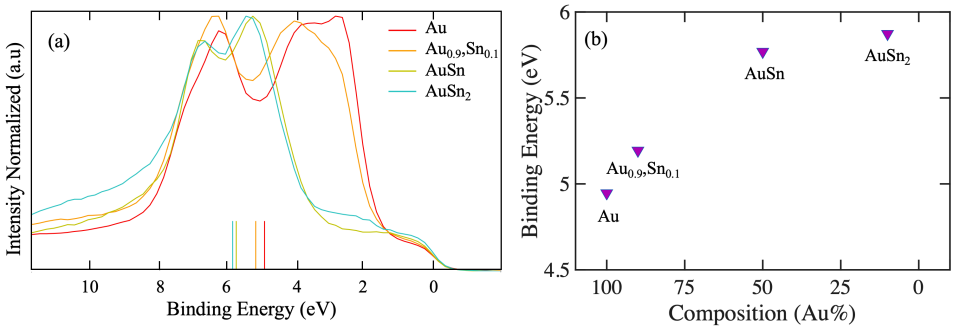

Figure 3.7: *Change in partial current density with composition at constant current density.*

The position of the d-band center is indicative of the strength of the bond between the metal and the adsorbate. The closer the d-band center to the fermi energy level, the more empty the antibonding states, which leads to a stronger adsorption bond.[39] From Figure 3.7, it can be seen that the d- band center of Au is closest to the Fermi energy level, and Au is known to have weak binding energy for *COOH and *CO,[40] which leads to optimal conditions for the conversion of CO_2 to CO. With the increasing Sn content, the d-band center shifts further away from the fermi energy level, which may decrease the capability of the catalyst to support *COOH. The d-band center moves away from the fermi level, as the composition changes from pure Au to $AuSn_2$. Such a shift could result in the decrease in the selectivity to CO_2 reduction, which is what we observe. However, the shift of the d-band center does not show a linear decrease in the ability of the catalyst to reduce CO_2. In fact, after the initial drop in the FE for CO_2 reduction, the further addition of Sn increases the partial current density of CO and formate, while the HER decreases. The addition of Sn does seem to suppress the HER;[20] however, at lower Sn compositions, the electronic effect of the d-band shift dominates, diminishing the capability of CO_2 reduction to CO. The increasing Sn content also increases the amount of Sn

present on the surface of the catalysts. The increasing activity to CO_2 reduction could be due to the excess Sn on the surface.

Another possibility for the inactivity of the catalysts for CO_2 reduction could be due to the difference in composition at the surface of the catalysts, compared to the bulk. The Au/Sn phase present at the surface may be very different from that detected in the bulk with the XRD. This was confirmed for the $AuSn_2$ film, but conclusive data for the rest of the composition were not available. The presence of these different phases could possibly be inert to CO_2 reduction or present different binding energies for reaction intermediates, compared to the pure phases. Furthermore, if the surface of the films has a high degree of heterogeneity, grain boundaries[41] between phases may also present unique catalytic sites that are different from the parent materials themselves.

3.4. CONCLUSIONS

In this work, a detailed characterization of Au, Sn, and bimetallic Au/Sn thin films was performed, along with electrochemical CO_2 reduction. Different phases of AuSn were obtained, including a $Au_{0.9}$,$Sn_{0.1}$ film, as well as AuSn and $AuSn_2$ phases. It was observed that even though certain metals can be mixed to provide desirable outcomes in terms of selectivity and activity, this is not the case with every possible combination of metals. The loss in selectivity for CO with the addition of Sn can be attributed to the electronic effect of moving the d-band center of Au away from the fermi energy level. However, the final activity of the catalyst to reduce any amount of CO_2 was due to the excess Sn present at the surface of the catalysts, a structural effect. Based on our material characterization, it seems that the bimetallic systems constitute the bimetallic phases identified in the bulk, but the surfaces of these systems are capped off by a heterogeneous mix of the bimetallic system and SnO_x (Figure 3.4).

BIBLIOGRAPHY

[1] Eleanor D. Bates et al. “CO2 capture by a task-specific ionic liquid”. In: *Journal of the American Chemical Society* 124.6 (2002), pp. 926–927. ISSN: 00027863. DOI: 10.1021/ja017593d.

[2] Chun Yen Chen et al. “Cultivation, photobioreactor design and harvesting of microalgae for biodiesel production: A critical review”. In: *Bioresource Technology* 102.1 (2011), pp. 71–81. ISSN: 09608524. DOI: 10.1016/j.biortech.2010.06.159. URL: http://dx.doi.org/10.1016/j.biortech.2010.06.159.

[3] Ahmad Galadima and Oki Muraza. “Catalytic thermal conversion of CO2 into fuels: Perspective and challenges”. In: *Renewable and Sustainable Energy Reviews* 115.November 2017 (2019), p. 109333. ISSN: 18790690. DOI: 10.1016/j.rser.2019.109333. URL: https://doi.org/10.1016/j.rser.2019.109333.

[4] Y. Hori. “Electrochemical CO2 Reduction on Metal Electrodes”. In: *Modern Aspects of Electrochemistry*. Ed. by Constantinos G. Vayenas, Ralph E. White, and Maria E. Gamboa-Aldeco. New York, NY: Springer New York, 2008, pp. 89–189. ISBN: 978-0-387-49489-0. DOI: 10.1007/978-0-387-49489-0_3. URL: https://doi.org/10.1007/978-0-387-49489-0_3.

[5] Phil De Luna et al. “What would it take for renewably powered electrosynthesis to displace petrochemical processes?” In: *Science* 364.6438 (2019). ISSN: 10959203. DOI: 10.1126/science.aav3506.

[6] Wenlei Zhu et al. “Monodisperse Au nanoparticles for selective electrocatalytic reduction of CO2 to CO”. In: *Journal of the American Chemical Society* 135.45 (2013), pp. 16833–16836. ISSN: 15205126. DOI: 10.1021/ja409445p. arXiv: arXiv:1011.1669v3.

[7] Sheng Zhang, Peng Kang, and Thomas J. Meyer. “Nanostructured tin catalysts for selective electrochemical reduction of carbon dioxide to formate”. In: *Journal of the American Chemical Society* 136.5 (2014), pp. 1734–1737. ISSN: 00027863. DOI: 10.1021/ja4113885. arXiv: arXiv:1408.1149.

[8] Mulatu Kassie Birhanu et al. “Copper and Copper-Based Bimetallic Catalysts for Carbon Dioxide Electroreduction”. In: *Advanced Materials Interfaces* 1800919 (2018), pp. 1–34. ISSN: 21967350. DOI: 10.1002/admi.201800919.

[9] Chengzhen Chen et al. “Selective electrochemical CO ₂ reduction over highly porous gold films”. In: *J. Mater. Chem. A* 5 (2017), pp. 21955–21964. ISSN: 2050-7488. DOI: 10.1039/C7TA04983H. URL: http://xlink.rsc.org/?DOI=C7TA04983H.

[10] Ming Ma et al. “Selective and Efficient Reduction of Carbon Dioxide to Carbon Monoxide on Oxide-Derived Nanostructured Silver Electrocatalysts”. In: *Angewandte Chemie - International Edition* 55.33 (2016), pp. 9748–9752. ISSN: 15213773. DOI: 10.1002/anie.201604654.

[11] Maor F. Baruch et al. “Mechanistic Insights into the Reduction of CO ₂ on Tin Electrodes using in Situ ATR-IR Spectroscopy”. In: *ACS Catalysis* 5.5 (2015), pp. 3148–3156. ISSN: 2155-5435. DOI: 10.1021/acscatal.5b00402. URL: http://pubs.acs.org/doi/10.1021/acscatal.5b00402.

[12] Chang Hoon Lee and Matthew W. Kanan. “Controlling H+ vs CO2 Reduction Selectivity on Pb Electrodes”. In: *ACS Catalysis* 5.1 (2015), pp. 465–469. ISSN: 21555435. DOI: 10.1021/cs5017672.

[13] Recep Kas et al. “Electrochemical CO2reduction on Cu2O-derived copper nanoparticles: Controlling the catalytic selectivity of hydrocarbons”. In: *Physical Chemistry Chemical Physics* 16.24 (2014), pp. 12194–12201. ISSN: 14639076. DOI: 10.1039/c4cp01520g.

[14] Qi Lu et al. “A selective and efficient electrocatalyst for carbon dioxide reduction”. In: *Nature Communications* 5 (2014), pp. 1–6. ISSN: 20411723. DOI: 10.1038/ncomms4242. arXiv: arXiv:1011.1669v3.

[15] Min Liu et al. “Enhanced electrocatalytic CO2 reduction via field-induced reagent concentration”. In: *Nature* 537.7620 (2016), pp. 382–386. ISSN: 14764687. DOI: 10.1038/nature19060. URL: http://dx.doi.org/10.1038/nature19060.

[16] Makoto Todoroki et al. “Electrochemical reduction of high pressure CO 2 at Pb, Hg and In electrodes in an aqueous KHCO 3 solution”. In: *Journal of Electroanalytical Chemistry* 394.1-2 (1995), pp. 199–203. ISSN: 00220728. DOI: 10.1016/0022-0728(95)04010-L.

[17] Akihiko Kudo et al. “Electrochemical Reduction of High Pressure CO2 on Ni Electrodes”. In: *Journal of the Electrochemical Society* 140.6 (1993), pp. 1541–1545. ISSN: 19457111. DOI: 10.1149/1.2221599.

[18] Yihong Chen and Matthew W. Kanan. “Tin oxide dependence of the CO 2 reduction efficiency on tin electrodes and enhanced activity for tin/tin oxide thin-film catalysts”. In: *Journal of the American Chemical Society* 134.4 (2012), pp. 1986–1989. ISSN: 00027863. DOI: 10.1021/ja2108799.

[19] Taotao Zhang et al. “Zn electrode with a layer of nanoparticles for selective electroreduction of CO 2 to formate in aqueous solutions”. In: *J. Mater. Chem. A* 4 (2016), pp. 16670–16676. ISSN: 2050-7488. DOI: 10.1039/C6TA07000K.

[20] Ming Ma et al. “Electrochemical Reduction of CO 2 on Compositionally Variant Au-Pt Bimetallic Thin Films”. In: *Nano Energy* 42.September (2017), pp. 51–57. ISSN: 22112855. DOI: 10.1016/j.nanoen.2017.09.043. URL: http://linkinghub.elsevier.com/retrieve/pii/S2211285517305827.

[21] Kai Liu et al. “Electronic Effects Determine the Selectivity of Planar Au-Cu Bimetallic Thin Films for Electrochemical CO 2 Reduction”. In: *ACS Applied Materials and Interfaces* 11.18 (2019), pp. 16546–16555. ISSN: 19448252. DOI: 10.1021/acsami.9b01553.

[22] Marco Valenti et al. “Suppressing H 2 Evolution and Promoting Selective CO 2 Electroreduction to CO at Low Overpotentials by Alloying Au with Pd”. In: *ACS Catalysis* 9.4 (2019), pp. 3527–3536. ISSN: 21555435. DOI: 10.1021/acscatal.8b04604.

[23] Dohyung Kim et al. “Synergistic geometric and electronic effects for electrochemical reduction of carbon dioxide using gold–copper bimetallic nanoparticles”. In: *Nature Communications* 5.May (2014), p. 4948. ISSN: 2041-1723. DOI: 10.1038/ncomms5948. arXiv: 9809069v1 [arXiv:gr-qc]. URL: http://www.nature.com/doifinder/10.1038/ncomms5948.

[24] Shahid Rasul et al. “A highly selective copper-indium bimetallic electrocatalyst for the electrochemical reduction of aqueous CO2to CO”. In: *Angewandte Chemie - International Edition* 54.7 (2015), pp. 2146–2150. ISSN: 15213773. DOI: 10.1002/anie.201410233. arXiv: 0402594v3 [arXiv:cond-mat].

[25] J. Christophe, Th Doneux, and C. Buess-Herman. “Electroreduction of Carbon Dioxide on Copper-Based Electrodes: Activity of Copper Single Crystals and Copper-Gold Alloys”. In: *Electrocatalysis* 3.2 (2012), pp. 139–146. ISSN: 18682529. DOI: 10.1007/s12678-012-0095-0.

[26] Cheonghee Kim et al. “Alloy Nanocatalysts for the Electrochemical Oxygen Reduction (ORR) and the Direct Electrochemical Carbon Dioxide Reduction Reaction (CO 2 RR)”. In: 1805617 (2018), pp. 1–19. DOI: 10.1002/adma.201805617.

[27] Ahmed Mohsen Ismail et al. “Composition Dependent Electrocatalytic Behavior of Au– Sn Bimetallic Nanoparticles in Carbon Dioxide Reduction”. In: *ACS Energy Letters* 4.1 (2019), pp. 48–53. ISSN: 23808195. DOI: 10.1021/acsenergylett.8b01996. URL: http://pubs.acs.org/doi/10.1021/acsenergylett.8b01996.

[28] Goran S. Matijasevic, Chin C. Lee, and Chen Y. Wang. “AuSn alloy phase diagram and properties related to its use as a bonding medium”. In: *Thin Solid Films* 223.2 (1993), pp. 276–287. ISSN: 00406090. DOI: 10.1016/0040-6090(93)90533-U.

[29] H. Kandler P. Eckerlin. *Structure Data of Elements and Intermetallic Phases Landolt-Börnstein - Group III Condensed Matter*. Ed. by A. M. Hellwege K.-H. Hellwege. ISBN: 978-3-540-36859-5. DOI: 10.1007/b19971.

[30] H. Okamoto and T. B. Massalski. “The Au-Sn (Gold-tin) system”. In: *Bulletin of Alloy Phase Diagrams* 5.5 (1984), pp. 492–503. ISSN: 01970216. DOI: 10.1007/BF02872904.

[31] H. M. Maltanava, O. N. Vrublevskaya, and T. N. Vorobyova. “Electrochemical deposition of gold-tin alloy from propyleneglycol electrolyte”. In: *Metal Finishing* 111.6 (2013), pp. 28–34. ISSN: 00260576. DOI: 10.1016/S0026-0576(13)70282-4. URL: http://dx.doi.org/10.1016/S0026-0576(13)70282-4.

[32] A. Debski et al. “Enthalpy of formation of intermetallic phases from the Au-Sn system”. In: *Journal of Alloys and Compounds* 491.1-2 (2010), pp. 173–177. ISSN: 09258388. DOI: 10.1016/j.jallcom.2009.11.003.

[33] Vincent Grolier and Rainer Schmid-fetzer. “Thermodynamic evaluation of the Au – Sn system”. In: 98 (2007), pp. 797–806.

[34] Song Yi Choi et al. “Electrochemical Reduction of Carbon Dioxide to Formate on Tin-Lead Alloys”. In: *ACS Sustainable Chemistry and Engineering* 4.3 (2016), pp. 1311–1318. ISSN: 21680485. DOI: 10.1021/acssuschemeng.5b01336.

[35] O. Renault et al. “High-resolution XPS spectromicroscopy study of micro-patterned gold-tin surfaces”. In: *Applied Surface Science* 258.24 (2012), pp. 10077–10083. ISSN: 01694332. DOI: 10.1016/j.apsusc.2012.06.078. URL: http://dx.doi.org/10.1016/j.apsusc.2012.06.078.

[36] D L Perry, J Ashley Taylor, and Sailesh M Merchanta. “Study of the oxidation spectroscopy of gold-tin preforms using x-ray photoelectron”. In: *Journal of Applied Physics* 78.May 2002 (1995).

[37] Kailun Yang, Recep Kas, and Wilson A. Smith. “In Situ Infrared Spectroscopy Reveals Persistent Alkalinity near Electrode Surfaces during CO2 Electroreduction”. In: *Journal of the American Chemical Society* 141.40 (2019), pp. 15891–15900. ISSN: 15205126. DOI: 10.1021/jacs.9b07000.

[38] A. Nilsson et al. “The electronic structure effect in heterogeneous catalysis”. In: *Catalysis Letters* 100.3-4 (2005), pp. 111–114. ISSN: 1011372X. DOI: 10.1007/s10562-004-3434-9.

[39] J. K. Norskov et al. “Density functional theory in surface chemistry and catalysis”. In: *Proceedings of the National Academy of Sciences* 108.3 (2011), pp. 937–943. ISSN: 0027-8424. DOI: 10.1073/pnas.1006652108.

[40] Xinyan Liu et al. “Understanding trends in electrochemical carbon dioxide reduction rates”. In: *Nature Communications* 8 (2017). ISSN: 2041-1723. DOI: 10.1038/ncomms15438.

[41] Ruperto G. Mariano et al. “Selective increase in CO2electroreduction activity at grain-boundary surface terminations”. In: *Science* 358.6367 (2017), pp. 1187–1192. ISSN: 10959203. DOI: 10.1126/science.aao3691.

4

AgPd Alloys for CO_2 Reduction in MEA

The field of electrochemical CO_2 reductions has been transitioning to industrially relevant scales by changing the architecture of the electrochemical cells and moving away from the traditional aqueous H-Cells to Membrane Electrode Assemblies (MEA). The reaction environment in MEAs, vary drastically from that of aqueous H-cells, which could result in significantly different catalytic activity. In this paper we test AgPd alloys, one of the most promising CO producing catalysts reported, at industrially relevant scales (50 to 200 mA/cm^2) in a MEA configuration. We report that with increasing Pd composition in the electrode, the CO selectivity reduces from 99% for pure Ag to 73% for pure Pd at 50 mA/cm^2. The MEA configuration helps attain a high CO partial current density of 123 mA/cm^2. We find that catalytic activity reported in aqueous H-Cells does not translate at higher current densities and that cell architecture must play an important role in benchmarking catalytic activity.

4.1. Introduction

Electrochemical CO_2 Reduction (ECO_2R) has gained significant interest in the past decades for its prospective role in contributing to a net-zero CO_2 society. The electrochemical conversion of CO_2 can produce valuable chemical feedstocks for the chemical industry such as CO,[1][2] formic acid[3][4] and ethylene,[5][6] By integrating this process with carbon capture technology and excess electricity generated by renewable sources, a potential net-zero carbon cycle can be established.

ECO_2R has been studied for decades in aqueous H-cell systems, and by varying parameters such as cathode composition,[7] electrolyte composition[5][8][9] and cell design,[10] it has been possible to tune the cathodic reactions to produce different products. The reaction pathways for each product vary, and have different material and operational factors that affect their activity and selectivity. Of these, catalyst composition and morphology have been the most studied by the research community, as they offer diverse platforms to tune and alter reaction selectivity. Combining two metals as alloys or bimetallic catalysts with varying ratios has provided some control on the products formed showing both synergistic and deleterious effects.[11][12][13][14] In these bimetallic catalysts, Au, Ag and Cu have been primarily chosen as at least one of the metals as they have shown high selectivities for different products (Ag and Au selectively make CO, whereas Cu can produce a wide range of C1 and C2 hydrocarbons).

Of particular interest in this work is the conversion of CO_2 to CO. Several combinations of metals in bimetallic and alloy catalysts have shown high selectivities for CO,[2][15][16] including AgPd alloys which have shown remarkably high selectivities for CO. Aqueous based H-Cell studies of AgPd alloys have shown its ability to outperform pure silver in their selective formation for CO.[16] Under cathodic potentials in aqueous environments, Pd has been shown to form the ß phase of its hydride which has a higher Gibbs free energy for CO adsorption as well as for the Volmer step in hydrogen evolution reaction (HER), which is proposed to be the reason for its high selectivity for ECO_2R compared to HER.[17] A similar effect has been observed with AgPd alloys where PdH forms a solid solution with Ag.[17][18] AgPd alloys have also been proposed as a candidate alloy that can approach the limit of the scaling relationship by lowering the adsorption energy for CO* more than that of COOH*.[16]

For ECO_2R to become integrated into industrial processes, a high selectivity (FE>90%) and activity (>200 mA/cm^2) for a single product and stability for multiple hours (>8000 hrs),[19] at reasonable cell potentials (< 3 V) are necessary.[19] Recently, research has focused on reactor configurations that have the ability to reach >200 mA/cm^2 using gas diffusion electrodes (GDEs) and membrane electrode assemblies (MEAs).[19][20]

Membrane electrode assemblies (Figure 4.1) are a zero-gap configuration where the anode, membrane and cathode are compressed together to form one reactor (Figure 4.1b). Gaseous CO_2 is directly fed to the electrode where it can diffuse through a porous transport layer to the catalyst surface. This zero-gap configuration allows for a very low resistance between the electrodes, while the high concentration of CO_2 helps in achieving the required high current densities. While this configuration is beneficial for scaling up this technology, it creates a reaction environment that is very different from what is found in a conventional H-cell where most catalyst screening and mechanistic insights have been gained. High current densities, attainable in GDE cells and MEAs, will signif-

icantly alter the local pH, changing the catalyst activity, selectivity and durability, while also requiring a different applied potential than for purely aqueous systems. The presence of an electrolyte membrane in direct contact with the catalyst also will affect the catalyst behavior compared to a traditional catalyst-liquid electrolyte interface.

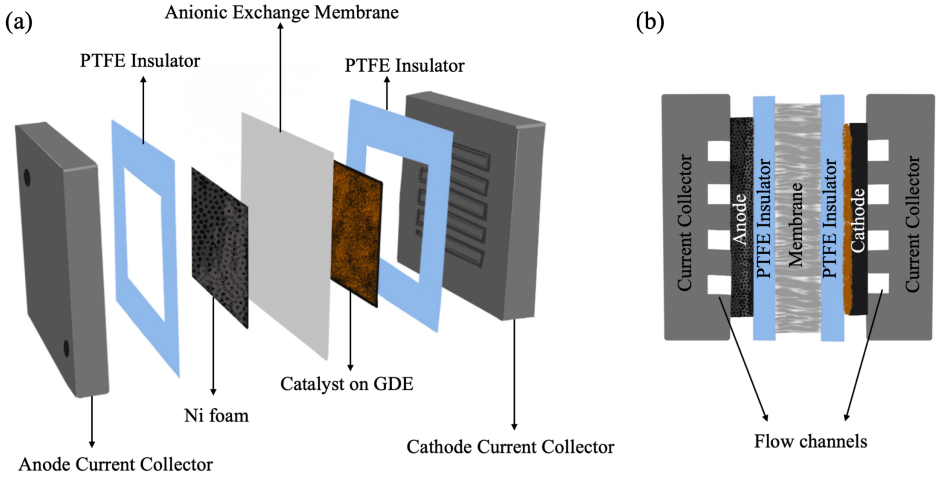

Figure 4.1: *(a) Schematic representation of a MEA, (b) Cross-sectional view of an assembled MEA.*

In this paper we use an MEA electrolyser to study one of the most promising silver alloy catalysts for CO_2 reduction, AgPd, at higher current densities than previously assessed.[16][18] Compositionally variant thin films were deposited by magnetron sputtering onto GDEs and used as catalysts and tested at current densities up to 200 mA/cm^2. The catalytic activity was found to be significantly different compared to activity reported in low current density configurations, showing the importance of screening catalysts at industrially relevant current densities and the need to bridge fundamental and applied studies of catalysts. CO selectivity is lost with increasing the Pd ratio, and is suspected to be due to the architecture of the MEA cell, emphasizing the need for catalyst design and testing at high current densities with various cell architectures.

4.2. EXPERIMENTAL METHODS

Sample Preparation. RF magnetron co-sputtering was used to deposit thin films of various Ag and Pd compositions onto GDEs (Sigracet 39BC) based on the method published previously.[21] The composition of the thin films was controlled by varying the DC power supplied to the pure Ag (99.99%, MaTeck GmbH) and Pd (99.99%, MaTeck GmbH) metal targets, and the thickness was controlled by the duration of the sputtering (150 nm) and checked by a quartz crystal microbalance (QCM). Each electrode had a total geometric area of 6.25 cm^2. The different powers supplied and the expected compositions are detailed in the Supporting Information (Appendix C, Table C.1).

Material Characterization. X-Ray Diffraction (XRD) patterns (30°–80°2θ) for the as-prepared samples were collected by a Bruker D8 Advance X-ray diffractometer using a cobalt source (γ = 1.7889 Å) in Bragg–Brentano configuration. After electrolysis, another diffractogram of the samples was taken to note any changes. X-Ray Photoelectron Spectroscopy (XPS) experiments were conducted using a Thermo Scientific K-alpha apparatus equipped with an Al K-alpha X-ray Source and a flood gun to avoid charging of the sample. Parameters used for the measurements were: spot size of 400 μm, pass energy of 50 eV, energy step size of 0.1 eV, dwell time of 50 ms, 10 scans in the vicinity of Ag 3d, Pd 3d, O 1s and C 1s orbital binding energies. To obtain valence band spectra, the number of scans was increased to 100. XPS spectra were corrected using the 1s peak from atmospheric carbon (284.8 eV).

Electrochemistry. The electrochemical conversion was conducted in a commercially available MEA setup from Dioxide Materials. Ni metal foam (Recemat BV) was used as the anode and an anion exchange membrane (AEM) (Sustainion, Dioxide Materials)[22] was placed between the anode and cathode. CO_2 was humidified upstream to the MEA and fed to the cathode at 30 ml/min. 1M KOH was fed to the anode at 20 ml/min from a 100 ml reservoir, to maintain a constant pH of the anolyte. Such a high flowrate of anolyte was required to efficiently remove gas bubbles formed in the Ni foam. Experiments were conducted by applying a constant current density (50, 100, 150, 200 mA/cm^2) and measuring the potential over the span of 60 minutes. A new membrane electrode assembly was constructed each time with a fresh cathode and Sustainion membrane. The Ni metal foam was reused for the entire data set. The gas stream exiting the cathode was analyzed every 10 min by an online Gas Chromatograph (GC) (Compact GC 4.0, GAS) with an internal N_2 reference.

4.3. Results and Discussion

To test the electrochemical performance of the AgPd alloys within a MEA architecture, it was necessary to synthesize compositionally variant catalysts on gas diffusion layers. Three compositionally variant thin film alloys of Ag and Pd along with pure Ag and Pd as control samples were fabricated on GDEs and characterized for their morphological, electronic and compositional properties. The three intermediate compositions chosen for synthesis were $Ag_{75}Pd_{25}$, $Ag_{50}Pd_{50}$, $Ag_{25}Pd_{75}$. The following subsections discuss the material characterization of these thin films followed by their electrocatalytic performance as CO_2 reduction catalysts.

4.3.1. Material Characterisation

Electrodes were characterized before and after electrolysis using XRD and XPS (Figure 4.2). XRD provides information on the bulk crystal structure of the material whereas XPS provides information over the surface composition of the catalysts along with information about metal orbital energy levels.

Figure 4.2 (a,b) shows the XRD patterns obtained for the as synthesized Ag, $Ag_{75}Pd_{25}$, $Ag_{50}Pd_{50}$, $Ag_{25}Pd_{75}$ and Pd. The patterns can be identified as a face centered cubic (fcc)

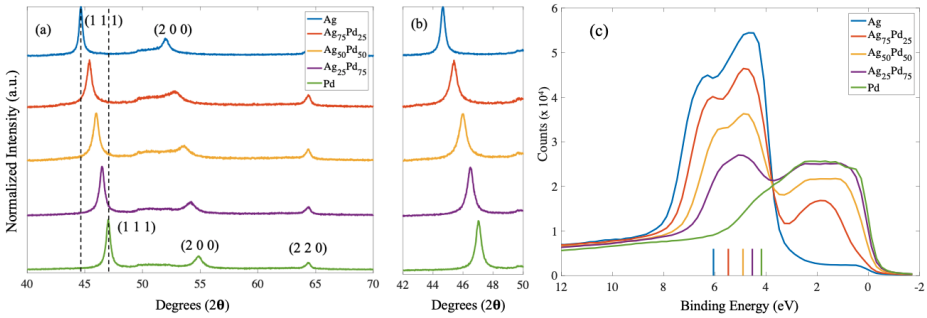

Figure 4.2: *((a and b) X-ray diffraction pattern of the different compositions synthesized, (c) Valence band spectra.*

system with (111), (200) and (220) facets being prominent for the pure Ag and Pd samples. The peaks of the intermediate compositions lie in between that of the pure metals showing the formation of alloys.[16][23] The main peak (111), shifts from 44.7°for Ag to 47.0°for Pd (Figure 4.2b), indicating the contraction of the lattice upon introducing the smaller Pd atoms (The calculated compositions using Vegard's Law are documented in Appendix C, Table C.2, including the change in lattice parameters).

The electrodes were also characterized after electrolysis for 60 min (Appendix C, Figure C.1) where the ex-situ analysis depicted no splitting of the main peaks, which suggests no phase segregation occurred during ECO_2R. The appearance of additional peaks as compared to the pre-electrolysis samples can be attributed to salt formation during electrolysis in the MEA configuration (Appendix C, Figure C.1).Salts are formed at elevated current densities in such configurations due to the interaction of OH^- and CO_2, leading to the production of HCO_3^- and CO_3^- ions and eventual precipitation upon interaction with K^+ (Equations 3.1,3.2,3.3).

$$CO_2 + H_2O + 2e^- \rightarrow CO + 2OH^- \tag{4.1}$$

$$CO_2 + OH^- \Longleftrightarrow HCO_3^- \tag{4.2}$$

$$HCO_3^- + OH^- \Longleftrightarrow {CO_3}^{2-} + H_2O \tag{4.3}$$

Low conductivity of these ions through the anion exchange membrane (AEM) and an increased conduction of co-ions (such as K^+) from the anolyte promotes the formation of salt in and on the surface of the GDE. This can be seen with the increasing intensity of the $KHCO_3$ salt peaks with increasing current density (Appendix C, Figure C.1). These salt formations are also visible in the SEM images taken of the catalyst surface after electrolysis (Appendix C Figure C.6 – C.10). The SEM images also show increasing salt deposits on the catalyst surface with increasing current densities. At higher current densities (200 mA/cm^2) the salt penetrated the GDE and deposited in the cathode flow channel blocking the flow of CO_2 and increasing the upstream pressure. This highlights

the importance and need for better water and ion management in CO_2 electrolysis systems in general.[19][24][25][26]

The XPS spectra of the 3d orbitals of Ag and that of Pd are depicted in Figure C.2. Figure 4.2c depicts the valence band structures of the alloys and pure metals, obtained from XPS. The bars at the bottom of the graph show the position of the d-band centers of the different compositions. As the concentration of Pd increased, an amalgamation of the valence band structures was observed. The d-band center shifts closer to the fermi energy level with increasing Pd concentration, from 6 eV for Ag to 4.2 eV for Pd, a trend that has been previously observed.[16] Shifts in the peaks are attributed to the overlapping of bands in the metal atoms. Pd has shown a high affinity towards CO binding which is attributed to the position of its d-band center in the field of heterogeneous catalysis.[27]

The process of sputtering produces GDEs that are evenly covered by the metal imitating the morphology of the micropores layer underneath (Appendix C, Figure C.5). The SEM images (Appendix C, Figure C.5 – C.10) of the catalysts, taken before and after electrolysis do not show any morphological changes occurring due to electrolysis.

4.3.2. Electrochemical Measurements

Chrono-potentiometric experiments were conducted on the 5 electrode compositions described, for 60 minutes, and gaseous products were analyzed with an online GC every 10 min. After electrolysis at different current densities, most of the samples showed no signs of flooding except for the samples at 200 mA/cm^2 where small water droplets were seen to flow out of the cathode chamber. Product selectivity over the period of 60 minutes is depicted in the Appendix C (Figure C.11). For the pure Ag electrode, the major product formed was CO, with the only minor product detected being H_2. The high selectivity for CO decreased from 99.5% at 50 mA/cm^2 to 62.0% at 200 mA/cm^2, while H_2 selectivity increased from 0.6% at 50mA/cm^2 to 15.0% at 200mA/cm^2. As the ratio of Pd increased, the selectivity for CO decreased and H_2 increased. All the alloys progressively produced less CO than Ag, contrary to what has been shown in previous literature,[18][23] while pure Pd had by far the lowest selectivity for CO (Figure 4.3e). For pure Pd, at 50 mA/cm^2 CO selectivity was 73.0%, which reduced to 18% at 200mA/cm^2. Concomitantly selectivity for H_2 increased from 33% at 50mA/cm^2 to 87.8% at 200mA/cm^2.

For the pure Ag catalyst, other than at 50 mA/cm^2, the total faradaic efficiency (FE) for all other current densities did not add up to 100%. This may be due to the increase in selectivity for formate, as Ag has been known to produce formate at high current densities.[2][28] Direct liquid product analysis could not be conducted since there was no bulk liquid catholyte, and the suspected formate ions can easily cross over the AEM, where they can be oxidized to CO_2 at the anode.[2][29] The selectivity towards formate at the cost of CO is more likely at high cathodic potentials and high alkalinity as has been shown extensively in previous literature.[30][31] The loss in total FE was observed for other electrode compositions as well, albeit without a clear trend. It is not possible to ascertain if this is due to formate production in a MEA configuration, as a loss in total FE could also be due to H_2 absorption by the Pd.[32][33] For pure Pd, the total FE added up to almost 100% and hence it is highly likely that the Pd does not produce formate or

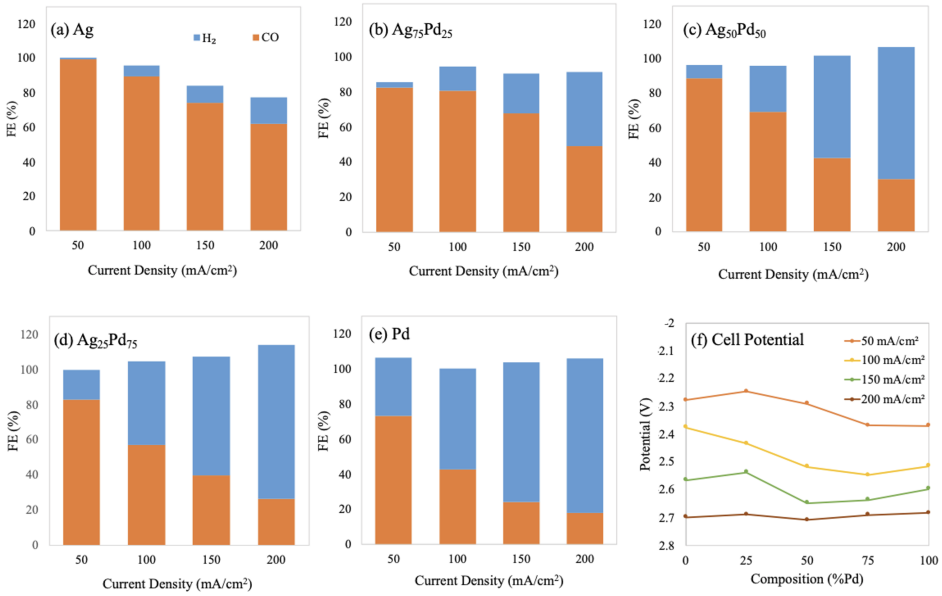

Figure 4.3: *Average faradaic efficiency measured (over 60 minutes) at different applied current densities at constant composition (a) Ag, (b) $Ag_{75}Pd_{25}$, (c) $Ag_{50}Pd_{50}$, (d) $Ag_{25}Pd_{75}$, (e) Pd and (f) Cell potentials of the different compositions at constant applied current densities.*

convert to PdH at these conditions.

Figure 4.3f shows the cell potentials needed to obtain the applied current densities for each sample composition. These values have been averaged over 60 minutes and the chrono-potentiometric curves can be found in Figure C.3. The cell potentials do not seem to have a strong dependence on the composition of the catalyst but rather on the current density applied. The cell potentials obtained here are relatively low for high current densities, as a current density of 200 mA/cm^2 was obtained at 2.7 V, depicting the advantage of using zero gap configuration for scaling up ECO_2R.

Figure 4.4 depicts the partial current densities (j) of CO (Figure 4.4a) and H_2 (Figure 4.4b) at different applied current densities. All the samples have similar j at 50 mA/cm^2 and diverge at higher current densities. The partial current density for CO is highest for pure Ag, and as the concentration of Pd increases in the catalyst the j_{CO} reaches a saturation point at lower and lower current densities. However, it was observed that the j_{CO} for Pd does not increase regardless of the applied current density. This could suggest poisoning of the Pd active sites by CO, that is not related to increasing the reaction rate.[18][23]

It is likely that the CO formed by ECO_2R at the start of the flow channel, poisons the

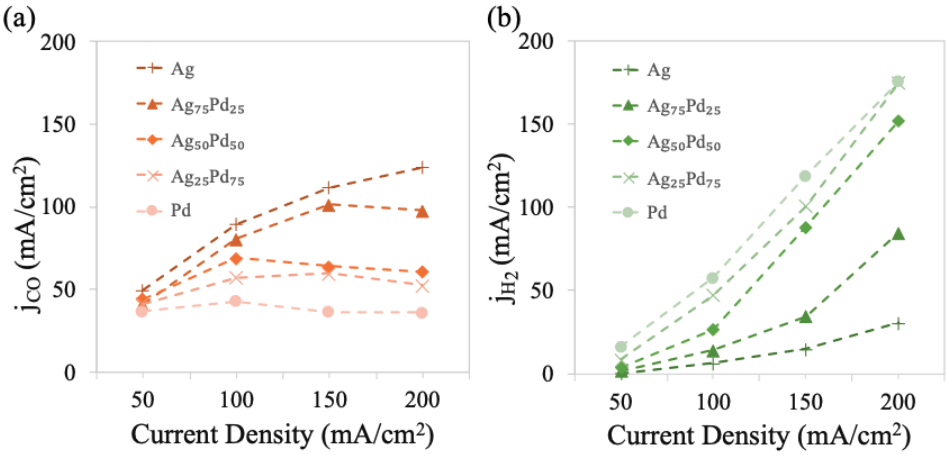

Figure 4.4: *a) Partial current density of CO and (b) H_2 as a function of applied current density (c) A schematic representation of the composition changing as the inlet gas flows through the cathode flow channel.*

rest of the Pd catalyst under negative applied potentials, as it flows through the rest of the flow channel. The presence of CO in the gas stream reaching the catalyst as it progresses through the channel could also inhibit H_2 adsorption, limiting the formation of PdH[34] (Figure 4.5), the formation of which has been thought to be the reason for the high CO selectivity seen on AgPd catalysts.[16][18] The chemisorbed CO has been proposed to block H_2 dissociation sites on Pd. As more Pd gets poisoned by CO, it produces more and more H_2 propelled by the higher selectivity for HER in alkaline conditions.[35][36] Reports suggesting PdH formation aided in the increase in selectivity towards CO were conducted in cell architectures very different from that used here.

In a MEA set up, using a serpentine flow channel for the gas reactant streams will alter its composition as it moves along the channel, much like a plug flow reactor (Figure 4.5). It is hence essential to understand the spatial activity of the catalyst as the reactant composition changes. Furthermore, previous reports did not see such plateauing behaviour of jCO on Pd, indicating that it could indeed be the MEA architecture that is responsible for the differences in activity and selectivity. More research conducted by monitoring the composition change of the gas streams at multiple points along the flow channel, and reporting current density and FE at these points rather than an average value base only on the outlet, will aid in designing better ECO_2R electrolysers.

At high current densities such as in our case, the slow kinetics for CO desorption[17] could lead to high concentrations of CO adsorbed on the surface inhibiting the formation of PdH and lowering the kinetics for CO_2 adsorption. The results presented here seem to indicate that while AgPd and PdH are suitable candidates for CO_2 reduction, this is limited to cases where the low current density and cell architecture do not allow

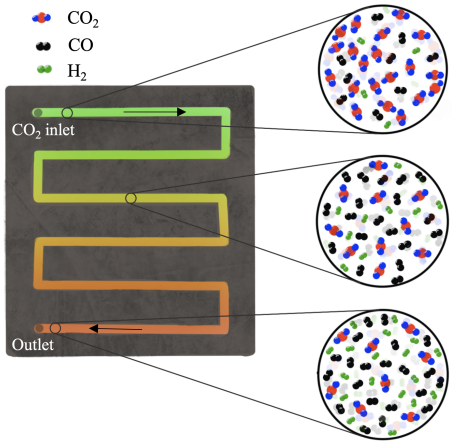

Figure 4.5: *Schematic diagram of the cathodic current collector depicting the change in composition of the reactant stream along the serpentine flow channel.*

for CO poisoning.

A carbon balance was calculated by using a N_2 internal reference to quantify the outlet products, along with the capability of the GC to quantify CO_2. This allowed for the calculation of the amount of CO_2 lost due to the cross over and the quantification of CO produced at the cathode. Figure 4.6a shows the outlet flowrate of CO from the cathode with a geometric surface area of 6.25 cm^2. Ag was capable of producing CO flowrates reaching up to 5.4 ml/min at 200 mA/cm^2. Pd produces the same amount of CO at all current densities, averaging around 1.65 ml/min.

Figure 4.6b shows the amount of CO_2 lost due to crossover of CO_3^-, HCO_3^-, and possibly $HCOO^-$. Which was measured by calculating the difference between the CO_2 in the inlet and the carbon products in the outlet. Under neutral and alkaline pH the protons for ECO_2R are provided by the water molecules, which leads to the conversion of CO_2 into carbonates[41] and bicarbonates which are capable of crossing the AEM to the anode (Equations 3.1-3.3). [37] It is also possible for any liquid products formed at the cathode to travel across the AEM to get oxidized at the anode to CO_2.[29] The amount of CO_2 lost due to crossover is heavily dependent on the current density applied, rather than the composition of the catalyst (Figure 4.6b). It is mainly the current density and CO_2 concentrations at the cathode that determine the amount of CO_2 crossing over for a particular membrane.[38] At a particular current density, the CO_2 lost to crossover is the same regardless of the composition. For Pd the loss may be slightly higher due to the higher concentrations of unreacted CO_2 at the catalyst surface. Calculating the percentage lost, about 10% of the CO_2 is lost due to crossover at 50 mA/cm^2 and as much as 35% is lost at 200 mA/cm^2. This loss of CO_2 to the anode is considerable under single pass conversions and could prove costly when scaling up as it is essentially the loss

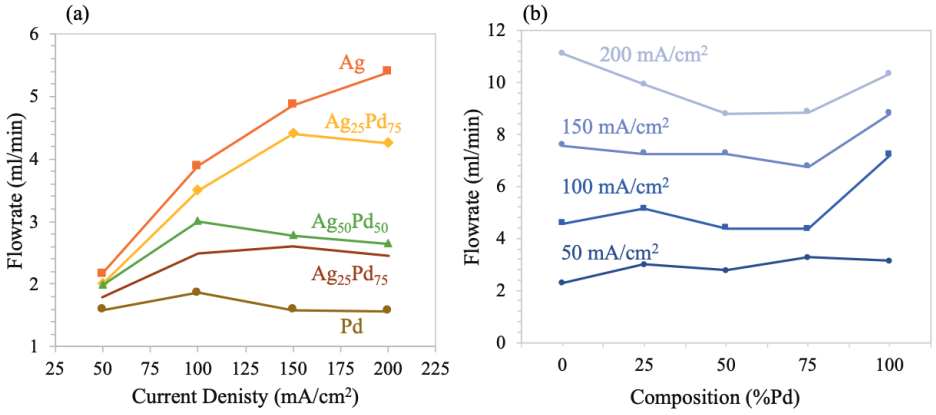

Figure 4.6: *(a) Flowrate of CO at the exit of cathode flow channel, (b) Average CO_2 flowrate lost due to crossover to the anode.*

of reactants. Minimizing CO_2 crossover has to be conjugated with handling excess carbonate and bicarbonate concentrations at the cathode. For this, membrane technology, catalyst design and cell design will have to be co-designed and supplement each other's optimization pathways.[37][29][39]

4.4. Conclusions

In this paper we examine the electrochemical operation of AgPd alloys at high current densities in an MEA configuration to perform ECO_2R. Unlike what has been reported about the success of AgPd catalysts at low current densities, the same activity has not been achieved at high current densities in this configuration. This may be due to the higher production rates of CO which poison the catalyst downstream of the CO inlet in the MEA. The use of a serpentine channel likely leads to CO contaminating a large part of the catalyst, inhibiting its activity. We also see that large quantities of CO_2 are lost due to membrane cross over, reducing the conversion rates of the set-up, regardless of the high current achieved. One of the reasons for the success of AgPd catalyst at low current densities was the position of the d-band center that promoted the selectivity for CO along with the formation of PdH. If the valence band theory can be applied to high current density situations also remains in question as it could be over ridden by the challenges brought on by the architecture of the MEA. It is with this knowledge that we need to encourage catalyst testing at high currents in the appropriate set ups in order to truly understand the effectiveness of the catalyst as a promising commercial catalyst.

BIBLIOGRAPHY

[1] Shuo Zhao, Renxi Jin, and Rongchao Jin. "Opportunities and Challenges in CO2 Reduction by Gold- and Silver-Based Electrocatalysts: From Bulk Metals to Nanoparticles and Atomically Precise Nanoclusters". In: *ACS Energy Letters* 3.2 (2018), pp. 452–462. ISSN: 23808195. DOI: 10.1021/acsenergylett.7b01104.

[2] Gastón O. Larrazábal et al. "Synergistic effects in silver–indium electrocatalysts for carbon dioxide reduction". In: *Journal of Catalysis* 343 (2016), pp. 266–277. ISSN: 10902694. DOI: 10.1016/j.jcat.2015.12.014.

[3] Maor F. Baruch et al. "Mechanistic Insights into the Reduction of CO ₂ on Tin Electrodes using in Situ ATR-IR Spectroscopy". In: *ACS Catalysis* 5.5 (2015), pp. 3148–3156. ISSN: 2155-5435. DOI: 10.1021/acscatal.5b00402. URL: http://pubs.acs.org/doi/10.1021/acscatal.5b00402.

[4] Song Yi Choi et al. "Electrochemical Reduction of Carbon Dioxide to Formate on Tin-Lead Alloys". In: *ACS Sustainable Chemistry and Engineering* 4.3 (2016), pp. 1311–1318. ISSN: 21680485. DOI: 10.1021/acssuschemeng.5b01336.

[5] Ana Sofia Varela. "The importance of pH in controlling the selectivity of the electrochemical CO2 reduction". In: *Current Opinion in Green and Sustainable Chemistry* 26 (Dec. 2020), p. 100371. DOI: 10.1016/j.cogsc.2020.100371.

[6] Ye Chen et al. "Ethylene Selectivity in Electrocatalytic CO2Reduction on Cu Nanomaterials: A Crystal Phase-Dependent Study". In: *Journal of the American Chemical Society* 142.29 (2020), pp. 12760–12766. ISSN: 15205126. DOI: 10.1021/jacs.0c04981.

[7] Jingfu He et al. "Electrocatalytic Alloys for CO2 Reduction". In: *ChemSusChem* 10 (2017), pp. 1–11. ISSN: 18645631. DOI: 10.1002/cssc.201701825. URL: http://doi.wiley.com/10.1002/cssc.201701825.

[8] Michael R. Thorson, Karl I. Siil, and Paul J.A. Kenis. "Effect of cations on the electrochemical conversion of CO2 to CO". In: *Journal of the Electrochemical Society* 160.1 (2013). ISSN: 00134651. DOI: 10.1149/2.052301jes.

[9] Kai Liu et al. "Electronic Effects Determine the Selectivity of Planar Au-Cu Bimetallic Thin Films for Electrochemical CO 2 Reduction". In: *ACS Applied Materials and Interfaces* 11.18 (2019), pp. 16546–16555. ISSN: 19448252. DOI: 10.1021/acsami.9b01553.

[10] Thomas Burdyny and Wilson A. Smith. "CO 2 reduction on gas-diffusion electrodes and why catalytic performance must be assessed at commercially-relevant conditions". In: *Energy & Environmental Science* 12 (2019), pp. 1442–1453. ISSN: 1754-5692. DOI: 10.1039/c8ee03134g.

[11] Shahid Rasul et al. “A highly selective copper-indium bimetallic electrocatalyst for the electrochemical reduction of aqueous CO2to CO”. In: *Angewandte Chemie - International Edition* 54.7 (2015), pp. 2146–2150. ISSN: 15213773. DOI: 10.1002/anie.201410233. arXiv: 0402594v3 [arXiv:cond-mat].

[12] Dohyung Kim et al. “Synergistic geometric and electronic effects for electrochemical reduction of carbon dioxide using gold–copper bimetallic nanoparticles”. In: *Nature Communications* 5.May (2014), p. 4948. ISSN: 2041-1723. DOI: 10.1038/ncomms5948. arXiv: 9809069v1 [arXiv:gr-qc]. URL: http://www.nature.com/doifinder/10.1038/ncomms5948.

[13] Ruud Kortlever et al. “Catalysts and Reaction Pathways for the Electrochemical Reduction of Carbon Dioxide”. In: *Journal of Physical Chemistry Letters* 6.20 (2015), pp. 4073–4082. ISSN: 19487185. DOI: 10.1021/acs.jpclett.5b01559.

[14] Sanjana Chandrashekar, Nathan T. Nesbitt, and Wilson A. Smith. “Electrochemical CO2Reduction over Bimetallic Au-Sn Thin Films: Comparing Activity and Selectivity against Morphological, Compositional, and Electronic Differences”. In: *Journal of Physical Chemistry C* 124.27 (2020), pp. 14573–14580. ISSN: 19327455. DOI: 10.1021/acs.jpcc.0c01894.

[15] Saad Sarfraz et al. “Cu-Sn Bimetallic Catalyst for Selective Aqueous Electroreduction of CO2to CO”. In: *ACS Catalysis* 6.5 (2016), pp. 2842–2851. ISSN: 21555435. DOI: 10.1021/acscatal.6b00269. arXiv: 0402594v3 [arXiv:cond-mat].

[16] Jiachang Zeng et al. “Pd - Ag Alloy Electrocatalysts for CO 2 Reduction: Composition Tuning to Break the Scaling Relationship”. In: *Applied materials and interfaces* 11.36 (2019), pp. 33074–33081. DOI: 10.1021/acsami.9b11729.

[17] Wenchao Sheng et al. “Electrochemical reduction of CO2 to synthesis gas with controlled CO/H2 ratios”. In: *Energy and Environmental Science* 10.5 (2017), pp. 1180–1185. ISSN: 17545706. DOI: 10.1039/c7ee00071e.

[18] Ji Hoon Lee et al. “Tuning the Activity and Selectivity of Electroreduction of CO2 to Synthesis Gas using Bimetallic Catalysts”. In: *Nature Communications* 10.28 (2019), pp. 1–8. ISSN: 2041-1723. DOI: 10.1038/s41467-019-11352-0. URL: http://dx.doi.org/10.1038/s41467-019-11352-0.

[19] David M. Weekes et al. “Electrolytic CO2 Reduction in a Flow Cell”. In: *Accounts of Chemical Research* 51.4 (Mar. 2018), pp. 910–918. DOI: 10.1021/acs.accounts.8b00010.

[20] Cao Thang Dinh et al. “CO2 electroreduction to ethylene via hydroxide-mediated copper catalysis at an abrupt interface”. In: *Science* 360.6390 (2018), pp. 783–787. ISSN: 10959203. DOI: 10.1126/science.aas9100.

[21] Ming Ma et al. “Electrochemical Reduction of CO 2 on Compositionally Variant Au-Pt Bimetallic Thin Films”. In: *Nano Energy* 42.September (2017), pp. 51–57. ISSN: 22112855. DOI: 10.1016/j.nanoen.2017.09.043. URL: http://linkinghub.elsevier.com/retrieve/pii/S2211285517305827.

[22] Robert B. Kutz et al. “Sustainion Imidazolium-Functionalized Polymers for Carbon Dioxide Electrolysis”. In: *Energy Technology* 5.6 (2017), pp. 929–936. ISSN: 21944296. DOI: 10.1002/ente.201600636.

[23] Takao Gunji et al. “Preparation of various pd-based alloys for electrocatalytic CO2reduction reaction - Selectivity depending on secondary elements”. In: *Chemistry of Materials* 32.16 (2020), pp. 6855–6863. ISSN: 15205002. DOI: 10.1021/acs.chemmater.0c01137.

[24] Y. Hori et al. “Silver-coated ion exchange membrane electrode applied to electrochemical reduction of carbon dioxide”. In: *Electrochimica Acta* 48.18 (2003), pp. 2651–2657. ISSN: 00134686. DOI: 10.1016/S0013-4686(03)00311-6.

[25] B. Smitha, S. Sridhar, and A. A. Khan. “Solid polymer electrolyte membranes for fuel cell applications - A review”. In: *Journal of Membrane Science* 259.1-2 (2005), pp. 10–26. ISSN: 03767388. DOI: 10.1016/j.memsci.2005.01.035.

[26] Jianan Erick Huang et al. “CO 2 electrolysis to multi-carbon products in strong acid”. In: *Science* 372 (2021), pp. 1074–1078.

[27] J. K. Norskov et al. “Density functional theory in surface chemistry and catalysis”. In: *Proceedings of the National Academy of Sciences* 108.3 (2011), pp. 937–943. ISSN: 0027-8424. DOI: 10.1073/pnas.1006652108.

[28] Toru Hatsukade et al. “Insights into the electrocatalytic reduction of CO2 on metallic silver surfaces”. In: *Physical Chemistry Chemical Physics* 16.27 (2014), pp. 13814–13819. ISSN: 14639076. DOI: 10.1039/c4cp00692e.

[29] Jie Zhang, Wen Luo, and Andreas Züttel. “Crossover of liquid products from electrochemical CO2 reduction through gas diffusion electrode and anion exchange membrane”. In: *Journal of Catalysis* 385 (2020), pp. 140–145. ISSN: 10902694. DOI: 10.1016/j.jcat.2020.03.013. URL: https://doi.org/10.1016/j.jcat.2020.03.013.

[30] Ezra L. Clark et al. “Influence of Atomic Surface Structure on the Activity of Ag for the Electrochemical Reduction of CO 2 to CO”. In: *ACS Catalysis* 9.5 (2019), pp. 4006–4014. ISSN: 21555435. DOI: 10.1021/acscatal.9b00260.

[31] Christine M. Gabardo et al. “Combined high alkalinity and pressurization enable efficient CO2 electroreduction to CO”. In: *Energy and Environmental Science* 11.9 (2018), pp. 2531–2539. ISSN: 17545706. DOI: 10.1039/c8ee01684d.

[32] Y. Hori. “Electrochemical CO2 Reduction on Metal Electrodes”. In: *Modern Aspects of Electrochemistry*. Ed. by Constantinos G. Vayenas, Ralph E. White, and Maria E. Gamboa-Aldeco. New York, NY: Springer New York, 2008, pp. 89–189. ISBN: 978-0-387-49489-0. DOI: 10.1007/978-0-387-49489-0_3. URL: https://doi.org/10.1007/978-0-387-49489-0_3.

[33] F. Lewis. “The Hydrides of Palladium and Palladium Alloys”. In: *Platinum Metals Review* 4.4 (1960), pp. 132–137. ISSN: 0032-1400.

[34] Casey P. O'Brien and Ivan C. Lee. "CO Poisoning and CO Hydrogenation on the Surface of Pd Hydrogen Separation Membranes". In: *Journal of Physical Chemistry C* 121.31 (2017), pp. 16864–16871. ISSN: 19327455. DOI: 10.1021/acs.jpcc.7b05046.

[35] Wenchao Sheng et al. "Correlating the hydrogen evolution reaction activity in alkaline electrolytes with the hydrogen binding energy on monometallic surfaces". In: *Energy and Environmental Science* 6.6 (2013), pp. 1509–1512. ISSN: 17545692. DOI: 10.1039/c3ee00045a.

[36] J. K. Nørskov et al. "Trends in the Exchange Current for Hydrogen Evolution". In: *Journal of The Electrochemical Society* 152.3 (2005), J23. DOI: 10.1149/1.1856988. URL: https://doi.org/10.1149/1.1856988.

[37] Gastón O. Larrazábal et al. "Analysis of Mass Flows and Membrane Cross-over in CO2 Reduction at High Current Densities in an MEA-Type Electrolyzer". In: *ACS Applied Materials and Interfaces* 11.44 (2019), pp. 41281–41288. ISSN: 19448252. DOI: 10.1021/acsami.9b13081.

[38] Noga Ziv, William E. Mustain, and Dario R. Dekel. "The Effect of Ambient Carbon Dioxide on Anion-Exchange Membrane Fuel Cells". In: *ChemSusChem* 11.7 (2018), pp. 1136–1150. ISSN: 1864564X. DOI: 10.1002/cssc.201702330.

[39] Lien Chun Weng, Alexis T. Bell, and Adam Z. Weber. "Towards membrane-electrode assembly systems for CO2 reduction: A modeling study". In: *Energy and Environmental Science* 12.6 (2019), pp. 1950–1968. ISSN: 17545706. DOI: 10.1039/c9ee00909d.

SUMMARY

The development of carbon dioxide sequestration and conversion technologies can help set up additional loops in the naturally occurring carbon cycle. It presents the unique opportunity to transition from a fossil fuel based industry to a CO_2 based industry. Life cycle analysis of CO_2 conversion processes which take into account the entire chemical conversion process have shown the advantages of using CO_2 as a source of chemicals. Coupling these technologies with renewable sources of energy such as solar and wind, will reduce the global warming impact (GWI), by reducing the total carbon content in the atmosphere and thus mitigating the climate disasters. These technologies can help ensure peoples lives are secured and that vulnerable cultures which are more dependent on nature are not washed away. It would help protect the lives of creatures who have no means of protection against the anthropological climate change.

The electrochemical conversion of carbon dioxide helps in setting up a carbon cycle, where CO_2 captured directly from the atmosphere or from point sources, is converted into basic industrial feedstock. This will allow industries to become less dependent on fossil fuels as their carbon source and move closer towards a net zero carbon cycle. A considerable amount of research has been conducted on how to control and optimize the electrochemical reduction of CO_2 in order for it to become a viable industrial technology. This pursuit has led to investigating various aspects of the technology such as the catalyst, the cell design and the electrolyte etc., to increase selectivity and activity towards a single CO_2 conversion product. This is key, since scaling up this technology will likely require CO_2 electrolysis to produce one single product to avoid extensive downstream processing.

The composition of the electrolyte and specifically the cations used, has been shown to have an effect on the activity and selectivity of the CO_2 reduction catalysts. By chelating the cations with cryptands in solution, it was possible to alter the way cations interact with the components of the electric double layer. The results of this study showed that cations play a very crucial role during CO_2 reduction. The absence of unchelated K^+ cations in the electrolyte appeared to completely suppress any CO_2 reduction. However by utilising surface enhanced infra-red spectroscopy (SEIRAS), we realized that CO_2 reduction was not completely suppressed but in fact continued to occur at very reduced scales. The role of cations during electrochemical CO_2 reduction appears to extend further than the stabilization of the adsorbed CO_2 molecule onto the catalyst. It was observed that cations also effect the absorption strengths of the products of CO_2 reduction. This opens up questions about the role of cations in during CO_2 conversion to C_2+ products and that more theoretical studies can no longer ignore the role of cations in the reaction mechanism.

The next work we conducted, studied AuSn bimetallic catalysts for CO_2 reduction in an H-Cell. Detailed characterization of AuSn bimetallic systems provided an opportunity to explain their activity for CO_2 conversion. XRD of the different compositions showed

that the Au and Sn did not form a homogeneous solid solution but instead formed a mixture of different phases. Using the phase diagram for the AuSn systems allowed us to identify these different phases. Depth analysis using XPS, where the thin film was slowly etched away in steps and the composition of these steps were analysed, showed that the thin films were all capped by a surface rich in Sn. Combining this knowledge with the product selectivites of the different compositions suggested that the none of the AuSn phases were very active for CO_2 conversion and that it was in fact the high Sn content at the surface that was orchestrating any observed CO_2 reduction. This is one of the many examples where catalyst characterization played a significant role in determining a structure functionality relationship between the catalyst and its catalytic activity. And as we continue to scale up this technology, catalyst development will still play an integral role.

In view of this, one of the most efficient reported CO producing catalyst, AgPd, was tested in a membrane electrode assembly. It became apparent that the activity of the catalysts in these systems do not translate from smaller scale ($< 5cm^2$). While studying AgPd alloys, a curious phenomena of constant CO partial current density on Pd catalysts regardless of the current density applied suggested that the CO produced at the start of the flow channel, poisoned the the Pd catalyst downstream, hence reducing its activity for CO_2 reduction. This can be attributed to the architectural changes to the electrochemical cell that are involved in achieving high current densities. All the implications of these changes are still yet unknown and will have to resolved as we progress towards a fully scaled up CO_2 electrolyser. This shows the need to for characterizing catalysts in high current density set ups and the need for a new bench-marking system.

The effects of electrolyte composition, catalyst composition and cell architecture were studied in this thesis. A fundamental study into the role of cations during CO_2 reduction showed that alkali cations must play an integral role in the reaction mechanism without which its makes CO_2 reduction very difficult to take place, and that further theoretical studies into the mechanism need to now actively consider the role of the cation. A lab scale study where test the activity of AuSn bimetallic catalysts and an industrial scale study on AgPd catalyst in MEAs. It is clear that is still a lot learn about the fundamentals of electrochemical reduction of CO_2 as well as the scaling up of the technology. However this must not hinder us from making progress towards scaling up this technology and study aspects that will ensure the implementation of this technology. As the conversion of CO_2 may not be the answer to all our problems because it is not a carbon sink, but still provides a more sustainable alternative to the current technology of using fossil fuels, and can definitely help contribute to the planet's health.

SAMENVATTING

De ontwikkeling van technologieën voor de vastlegging en omzetting van kooldioxide kan bijdragen tot het opzetten van extra kringlopen in de natuurlijk voorkomende koolstofcyclus. Het biedt de unieke kans om van een op fossiele brandstoffen gebaseerde industrie over te stappen op een op CO2 industrie. Levenscyclusanalyses van CO_2 omzettingsprocessen waarbij rekening wordt gehouden met het het gehele chemische omzettingsproces, hebben de voordelen aangetoond van het gebruik van CO_2 als bron van chemicaliën. Door deze technologieën te koppelen aan hernieuwbare energiebronnen zoals zonne- en windenergie, zal het effect op de opwarming van de aarde (GWI) verminderen, doordat het totale koolstofgehalte in de atmosfeer te verminderen en zo de klimaatrampen te verzachten. Deze technologieën kunnen helpen het leven van mensen veilig te stellen en te voorkomen dat kwetsbare culturen die meer afhankelijk zijn van de natuur, niet worden weggespoeld.

De elektrochemische omzetting van kooldioxide helpt bij het opzetten van een koolstofcyclus, waarbij CO_2 dat rechtstreeks uit de atmosfeer of uit puntbronnen wordt opgevangen, wordt omgezet in industriële basisgrondstof. Dit zal de industrie in staat stellen minder afhankelijk te worden van fossiele brandstoffen als hun koolstofbron en dichter in de buurt te komen van een koolstofcyclus met nuluitstoot. Er is een aanzienlijke hoeveelheid onderzoek verricht naar de wijze waarop de elektrochemische reductie van CO_2 kan worden beheerst en geoptimaliseerd, zodat dit een levensvatbare industriële technologie kan worden. Dit streven heeft geleid tot het onderzoeken van verschillende aspecten van de technologie, zoals de katalysator, het celontwerp en de elektrolyt, enz. om de selectiviteit en de activiteit op weg naar één enkel CO_2 omzettingsproduct te verhogen. Dit is van essentieel belang, aangezien voor het opschalen van deze technologie waarschijnlijk CO_2 elektrolyse nodig zal zijn om één enkel product te produceren, zodat geen uitgebreide downstream-verwerking nodig is.

Het is aangetoond dat de samenstelling van de elektrolyt, en meer bepaald de gebruikte kationen, een effect hebben op de activiteit en selectiviteit van de CO_2 reductiekatalysatoren. Door chelering van de kationen met crypto-elementen in oplossing was het mogelijk de wijze van interactie van de kationen met de componenten van de elektrische dubbele laag te wijzigen. De resultaten van deze studie toonden aan dat kationen een zeer cruciale rol spelen bij de CO_2 reductie. De afwezigheid van ongecheleerde K+ kationen in de elektrolyt bleek elke CO_2 reductie volledig te onderdrukken. Door gebruik te maken van oppervlakte versterkte infrarood spectroscopie (SEIRAS), realiseerden we ons echter dat CO_2 reductie niet volledig onderdrukt werd, maar in feite bleef plaatsvinden op zeer gereduceerde schaal. De rol van kationen tijdens elektrochemische CO2-reductie blijkt verder te gaan dan het stabiliseren van de geadsorbeerde CO_2 molecule aan de katalysator. Er werd waargenomen dat kationen ook de absorptiesterkte van de producten van de CO_2 reductie beïnvloeden. Dit doet vragen rijzen over de rol van kationen bij de omzetting van CO_2 in C_2+ producten en dat meer theoretische studies de

rol van kationen in het reactiemechanisme niet langer kunnen negeren.

Het volgende werk dat we hebben uitgevoerd, bestudeerde AuSn bimetaal katalysatoren voor CO_2 reductie in een H-Cel. Gedetailleerde karakterisering van AuSn bimetaal systemen gaf de mogelijkheid om hun activiteit voor CO_2 conversie te verklaren. XRD van de verschillende samenstellingen toonde aan dat Au en Sn geen homogene vaste oplossing vormden maar in plaats daarvan een mengsel van verschillende fasen. Met behulp van het fasediagram voor de AuSn systemen konden we deze verschillende fasen identificeren. Diepte-analyse met XPS, waarbij de dunne film langzaam in stappen werd weg geëtst en de samenstelling van deze stappen werd geanalyseerd, toonde aan dat de dunne films allemaal werden afgedekt door een oppervlak dat rijk was aan Sn. De combinatie van deze kennis met de productselectiviteit van de verschillende samenstellingen suggereerde dat geen van de AuSn fasen erg actief was voor CO_2 conversie en dat het in feite het hoge Sn gehalte aan het oppervlak was dat de waargenomen CO2 reductie orchestreerde. Dit is een van de vele voorbeelden waarbij de karakterisering van de katalysator een belangrijke rol heeft gespeeld bij het bepalen van de structuur-functionaliteit relatie tussen de katalysator en zijn katalytische activiteit. En naarmate we deze technologie verder opschalen, zal de ontwikkeling van katalysatoren nog steeds een integrale rol spelen.

Met het oog hierop werd een van de meest efficiënte CO-producerende katalysatoren, AgPd, getest in een membraan-elektrodeconstructie. Het werd duidelijk dat de activiteit van de katalysatoren in deze systemen zich niet vertaalt van kleinere schaal (5cm2). Bij het bestuderen van AgPd-legeringen deed een merkwaardig fenomeen van constante CO partiële stroomdichtheid op Pd-katalysatoren, ongeacht de toegepaste stroomdichtheid, vermoeden dat de CO die aan het begin van het stroomkanaal wordt geproduceerd, de Pd-katalysator stroomafwaarts vergiftigde, waardoor zijn activiteit voor CO_2 reductie verminderde. Dit kan worden toegeschreven aan de architectonische veranderingen in de elektrochemische cel die betrokken zijn bij het bereiken van hoge stromen dichtheden. Alle implicaties van deze veranderingen zijn nog onbekend en zullen moeten worden opgelost naarmate we vorderen in de richting van een volledig opgeschaalde CO_2 elektrolyser. Dit toont de de noodzaak van het karakteriseren van katalysatoren in opstellingen met hoge stroomdichtheid en de noodzaak van een nieuw benchmarking-systeem.

De effecten van de samenstelling van de elektrolyt, de samenstelling van de katalysator en de architectuur van de cel werden in dit proefschrift bestudeerd. Een fundamentele studie naar de rol van kationen tijdens CO_2 reductie toonde aan dat alkali kationen een integrale rol moeten spelen in het reactiemechanisme zonder welke CO2 reductie zeer moeilijk plaats kan vinden, en dat verdere theoretische studies naar het mechanisme nu actief rekening moeten houden met de rol van het kation. Een studie op laboratoriumschaal waarbij de activiteit van de bimetaalkatalysatoren AuSn wordt getest en een studie op industriële schaal van de AgPd- katalysator in MEA. Het is duidelijk dat is nog veel te leren valt over de grondslagen van elektrochemische reductie van CO_2, evenals als over de opschaling van de technologie. Dit mag ons er echter niet van weerhouden van het opschalen van deze technologie en het bestuderen van aspecten die de toepassing van deze technologie. De omzetting van CO_2 is misschien niet het antwoord voor al onze problemen, aangezien het geen koolstofput is, maar toch een duurzamer

alternatief voor de huidige technologie van het gebruik van fossiele brandstoffen, en zou kunnen helpen bij het beperken van klimaatrampen.

ACKNOWLEDGEMENTS

It is with quite contemplation that I write the next few words. Four years of PhD research is only possible with a healthy support system around you. These past years I have not walked alone, I have been surrounded by the kindest people constantly taking turns to lend me their hand. And it with their help that I have reached here.

This journey would not have been possible without **Wilson** deciding to give me chance at it. From the first day, I have loved how easy it is to have a conversation with you. We spoke about everything, our lives, our passions, our hobbies, and most importantly science. You made science so much fun with your giddy enthusiasm. It was not just about facts and figures, it was an adventure we took on every time I started a new project. It is why I enjoy science so much. You are a force beyond compare, with all that you care about. I know going forth in my life and career, knowing that I have been given the right tools from you to choose my own path and fight for what I care deeply about. Thank you, once again, for all that you have done. I could not have asked for a better supervisor.

Hans, we met a lot later in my PhD, but I am very glad I got to spend whatever time I could with you. In you, I found someone who would listen to me when I hit the rough patches and walk me through processing them. Your indignation at whatever was troubling me at any point was always soothing. Your grounding advice and your belief in me and my work has motivated me when I found it difficult to motivate myself. Thank you for all your help.
Thank you **Bernard** for checking in through out the PhD to help me make sure my work was on track. **Tom**, frankly, you are a huge part of what kept me sane during the crazy times. Your empathy and sage advise always calmed me down. You are my role model, in science and in life. Thank you for your faith in me and all your help.

Diana, my paranymph, it is weird how friendships begin but I truly glad ours did. Thank you always being there for a talk and listening to my ramblings the last couple of years. The kindness you show people is humbling. Have faith in yourself, you have such power in you. Believe it.
Marijn, we did indeed started our PhD on the same day (me an hour earlier, and since I say it last I win) and since then the more we got to know each other the more I valued our friendship. There is a lot I learned from you over the years. You had the unique capability to make any moment light. I am glad I was able to find you in some of those moments when I needed that the most

Kailun, all the time we spent together will be cherished. You and your amazing work ethics are going places. I wish you all the luck in the world.
The way friendships are made is a curious thing. **Hugo**, I do not know if it was the year

long struggle with SEIRAS that made me enjoy your company so much. But if it is, I would recommend it to everybody. Best of luck with your PhD, I am yet to meet someone as determined as you.

Mark, Markyyy, sweet sweet boy. From the bottom of my heart I wish you only happiness. Thank you for making lab time so lighthearted and fun.
Robin, I loved our coffee talks. They were cathartic, I needed them. Thank you. Miep and Vincent will always have a special place in my heart.
Nate, I think we made a great deal of progress during our discussion of my work over the pancakes. Thank you for being you and showing me life is not always so complicated. I am glad I get the opportunity to have more conversations with you over pancakes.
Divya I truly enjoyed our short tryst into the cation world. Should have done it more.
Giorgio and **Anirudh** Thank you for so many light-hearted moments, they were a relief.
Recep, all things said and done, I am grateful for all that you taught me and only wish you happiness. **Joost** and **Herman**, you always had magical solutions to my problems in the lab. You made sure that it was not just science that I was doing. **Sid**, thank you for your help with all things COMSOL.
Bart, thank you for your help with the XPS and for always having a smile. **Marcel**, those AFM days were gruelling but led to some amazing pictures. I am glad I had your guidance throughout. **Tom Savenije**, thank you for encouraging me to take this journey, I would not have had it any other way.

Maarten and **Michiel**, I learnt to conduct my electrochemical experiments under your guidance. The immense knowledge and experience you both have was humbling. I learnt so much more about CO_2 reduction from you than from papers. I loved our conversations on the problems we were facing and how to go about solving them. Thank you for sharing your knowledge and time with me. **Esther**, **Paul** and **Emanuela** thank you for enabling my research at STCA. I dont take it lightly the opportunity you gave me by allowing me to conduct research there. It gave me a very different outlook toward research.

Mama and **Papa**, thank you for your patience with me and my PhD. Thank you for letting this headstrong girl make her own choices. My journey has only been possible because of you. **Vishnu**, in you I found quite support, a comrade in arms who is always willing to try my latest cravings, I am surprised and glad. To my Grandfather, thank you for thinking ahead of your time. I wish you could have been here this day.

Tushar, T, my partner in food and all things good. Words fail me as I try to describe what your support has meant. I derive my strength from you, and I have needed it a lot these years. One single thank you wont suffice. I am glad I have the rest of my life to keep saying it.

A

APPENDIX A

Investigating the Role of Potassium Cations During Electrochemical CO_2 Reduction

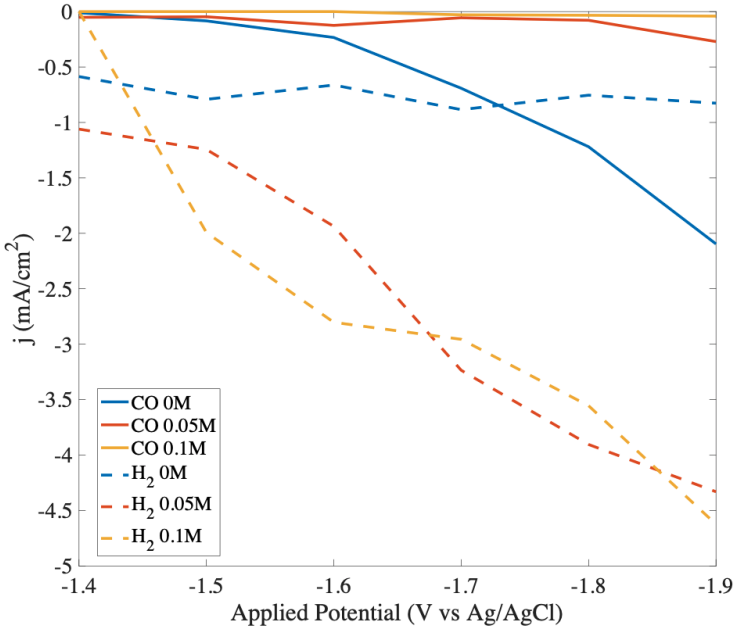

Figure A.1: *Partial current densities of CO and H_2 at increasing negative potentials, depicting the increase in partial current density of H_2 with increase in cryptand concentrations*

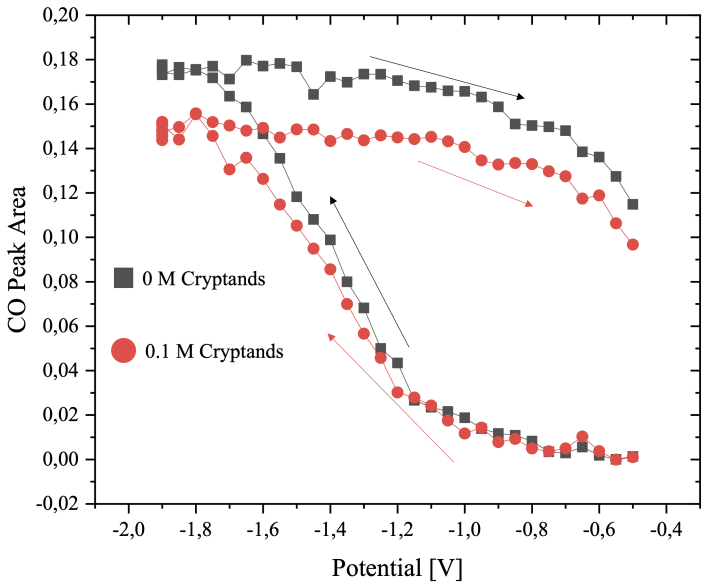

Figure A.2: *Forward and backward scans of CO at different concentrations of cryptands showing minimal difference in peak areas during backward scans*

B

APPENDIX B

Electrochemical CO2 Reduction Over Bimetallic Au-Sn Thin Films: Comparing Activity and Selectivity Against Morphological, Compositional and Electronic Differences

DC Power (Watt)		Expected Compositions
Au	Sn	
50	0	Au
38	10	$Au_{0.75}Sn_{0.25}$
12	29	$Au_{0.50}Sn_{0.50}$
11	50	$Au_{0.25}Sn_{0.75}$
0	20	Sn

Table B.1: DC power supplied to pure metal targets during catalyst synthesis and the expected compositions.

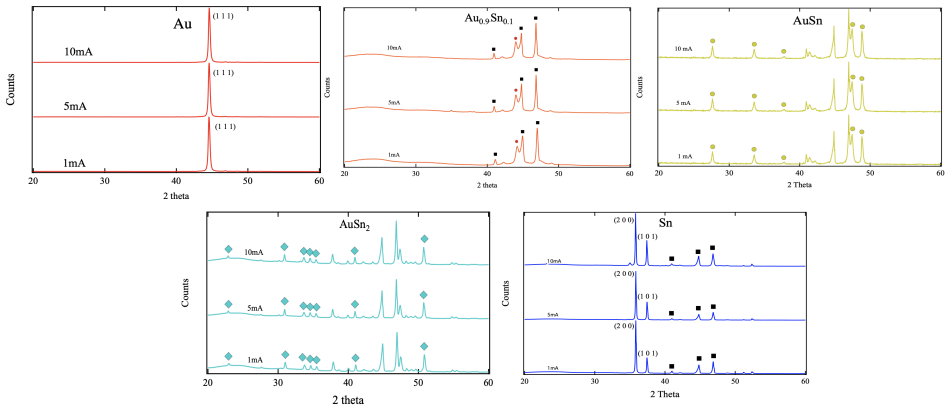

Figure B.1: *X-ray Diffractograms of the thin films after electrolysis.*

Looking at the XRD patterns obtained after electrolysis, it is interesting to note that each composition maintains its bulk structure at all current densities.

Composition	Au	AuSn	AuSn	AuSn	Sn
Ra (nm)	4.1	7.2	14.8	14.3	27.3

Table B.2: Roughness (Ra) of Samples before Electrolysis.

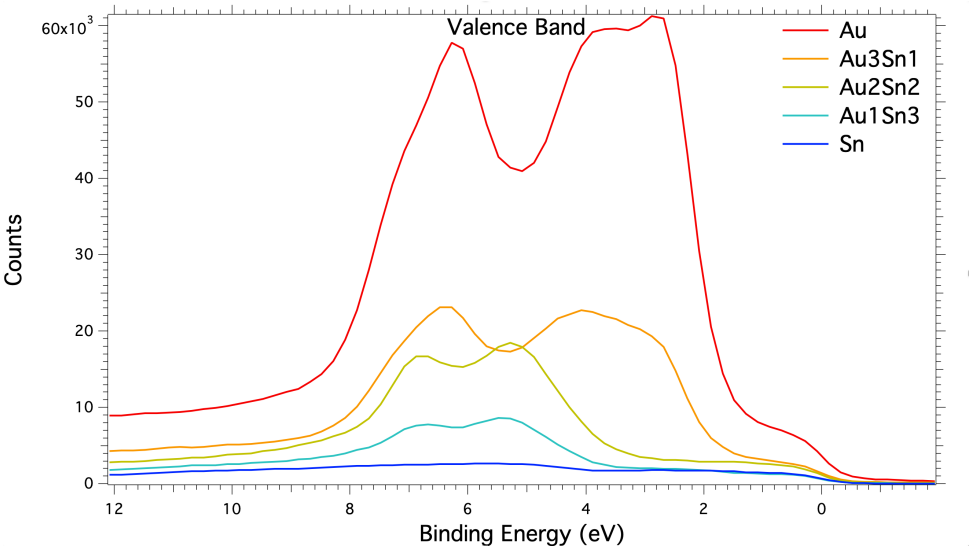

Figure B.2: *XPS Valence band spectra of Au, Au0.9,Sn0.1, AuSn, AuSn2, Sn*

The valence band structures were also measured to estimate the d-band energy of the catalysts as a function of composition, and the results are shown in Figure B.2. The intensity of the valence bands is indicative of the composition, we do not see distinctive valence bands of Sn in this particular graph as their intensity is much lower compared to that of Au. Taking into account the density of states between 0-12 eV. The metal d-band hybridizes with the bonding orbital of the adsorbate to form bonding and antibonding states. An increased filling of the antibonding state corresponds to a destabilization of the metal-adsorbate interaction. This leads to a weaker binding between the metal and the adsorbate. The experimentally-determinable parameter which correlates highly with the extent of filling of the antibonding MO is the location of the d-band center. The above figure depicts the normalized valence bands of the bimetallic compositions along with the pure metals. The d band center calculated using:

$$E_{\mathrm{d}} = \frac{\int N(\epsilon) * \epsilon * d\epsilon}{\int N(\epsilon) * d\epsilon} \tag{B.1}$$

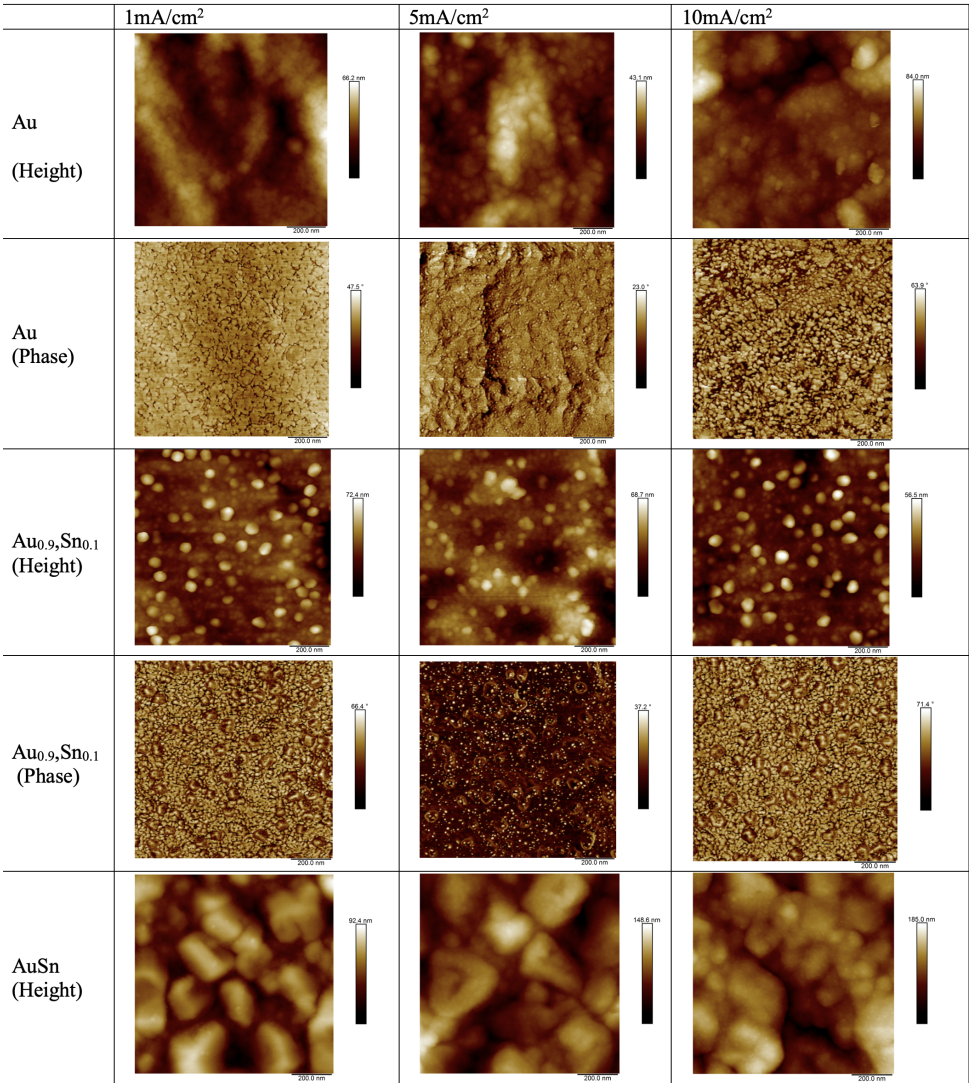

Figure B.3: *The AFM images obtained from the samples after electrolysis are depicted in the following table*

B

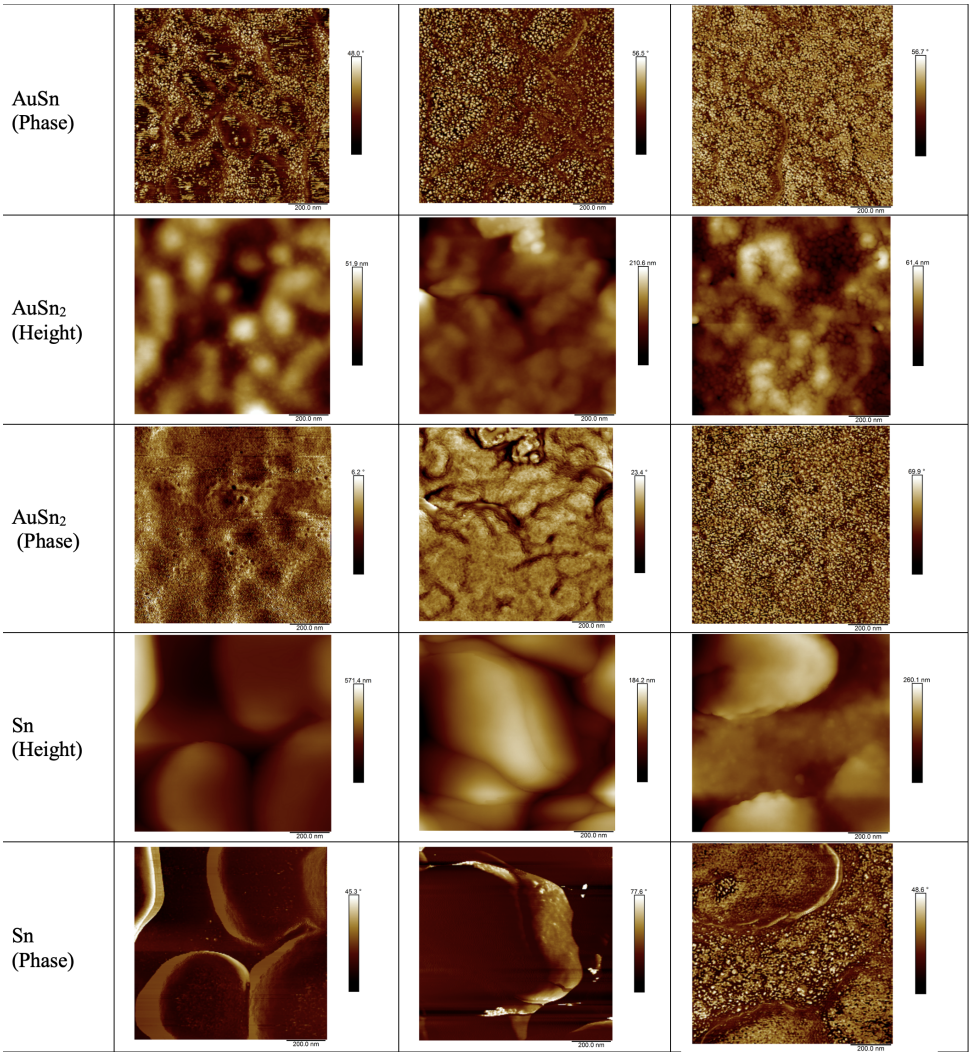

Figure B.4: *The AFM images obtained from the samples after electrolysis are depicted in the following table*

C

APPENDIX C

AgPd Alloys for CO_2 Reduction in MEA

DC Power Supplied (Watt)		Expected Composition (%)	
Ag	Pd	Ag	Pd
50	0	100	0
50	37	75	25
22	50	50	50
11	70	25	75
0	50	0	100

Table C.1: Power supplied to metal targets to obtain expected compositions.

Expected Composition	Lattice Parameter (nm)	Mole Fraction (Pd)	Mole Fraction (Ag)
Ag	1.27	0.00	1.00
$Ag_{75}Pd_{25}$	1.26	0.35	0.65
$Ag_{50}Pd_{50}$	1.24	0.58	0.42
$Ag_{25}Pd_{75}$	1.23	0.80	0.20
Pd	1.22	1.00	0.00

Table C.2: Calculated Lattice Parameters (Bragg's Law) and Calculated Composition (Vegard's Law).

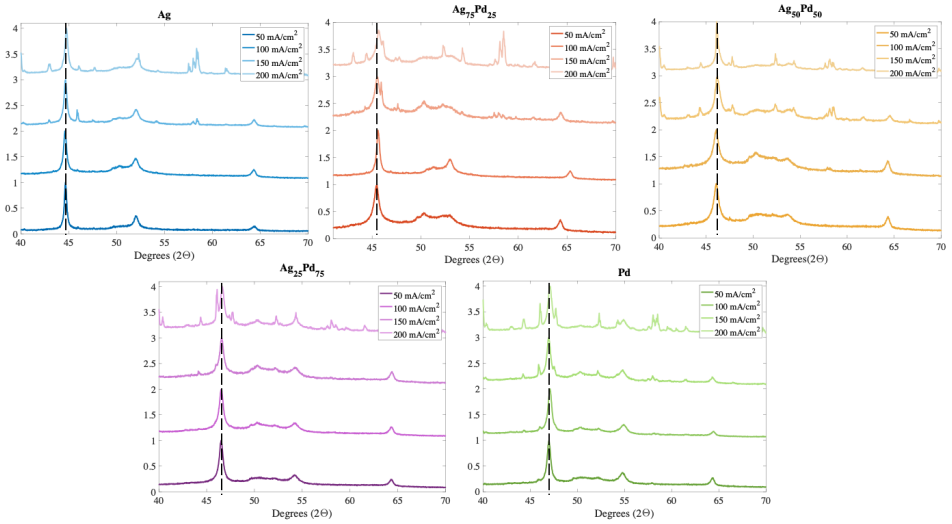

Figure C.1: *XRD Patterns of the different AgPd compositions taken after electrolysis.*

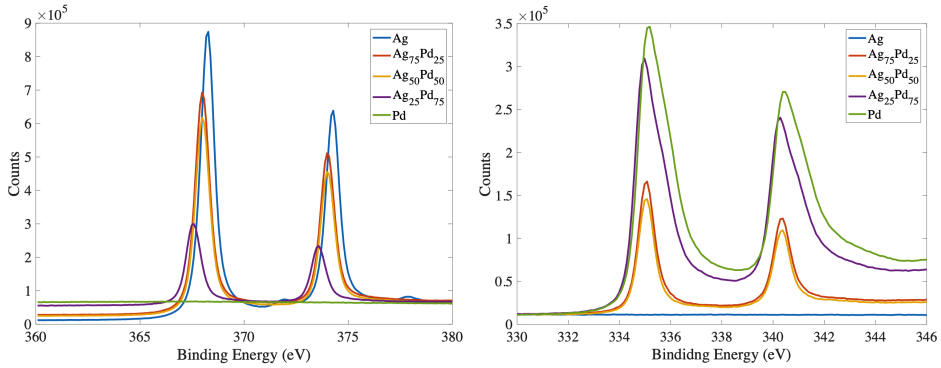

Figure C.2: *Ag 3d orbital scan and Pd 3d orbital scan.*

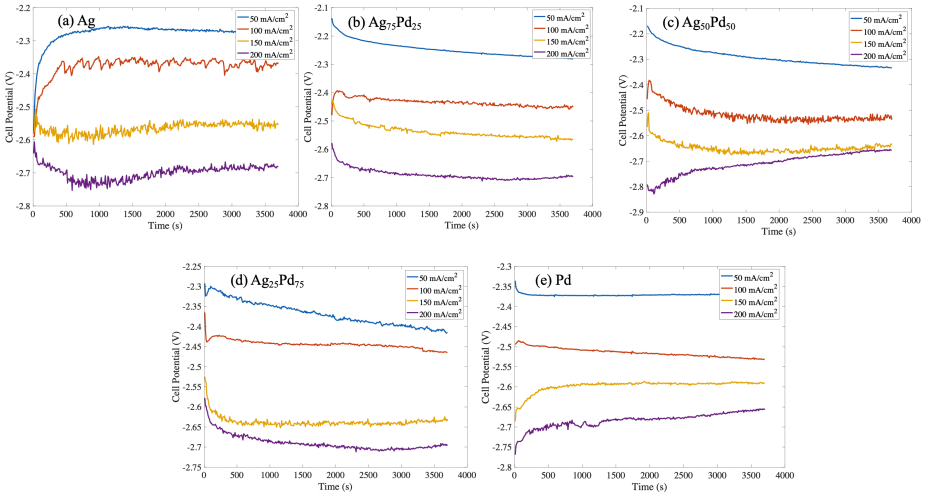

Figure C.3: *Chronopotentiometry curves at constant current densities of all the AgPd compositions.*

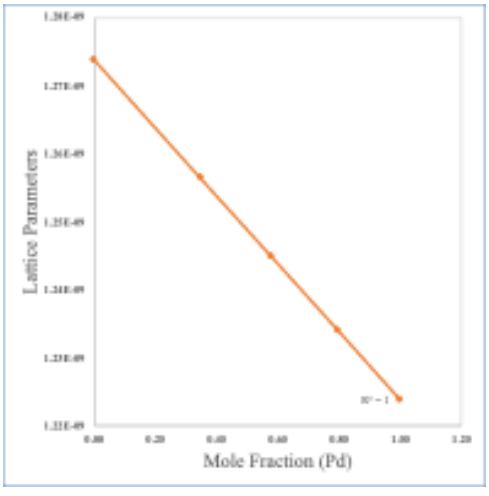

Figure C.4: *Lattice parameters plotted against composition to obtain bulk composition.*

C

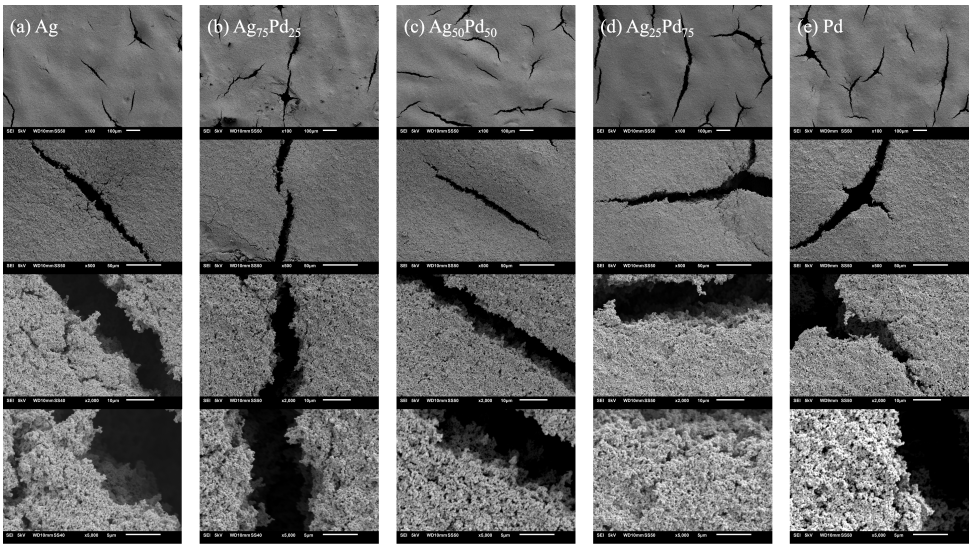

Figure C.5: *SEM images showing the morphology of the as synthesized catalyst layers on the GDEs.*

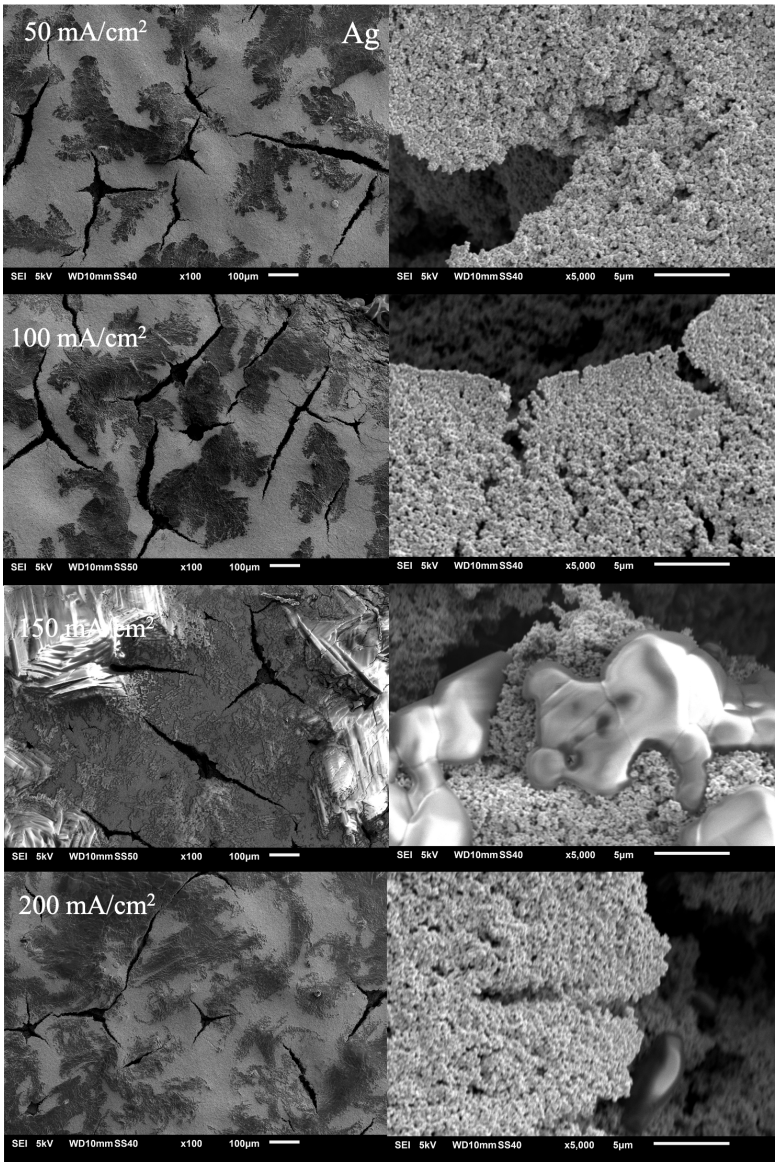

Figure C.6: *SEM images of the Ag surface after electrolysis at the different current densities.*

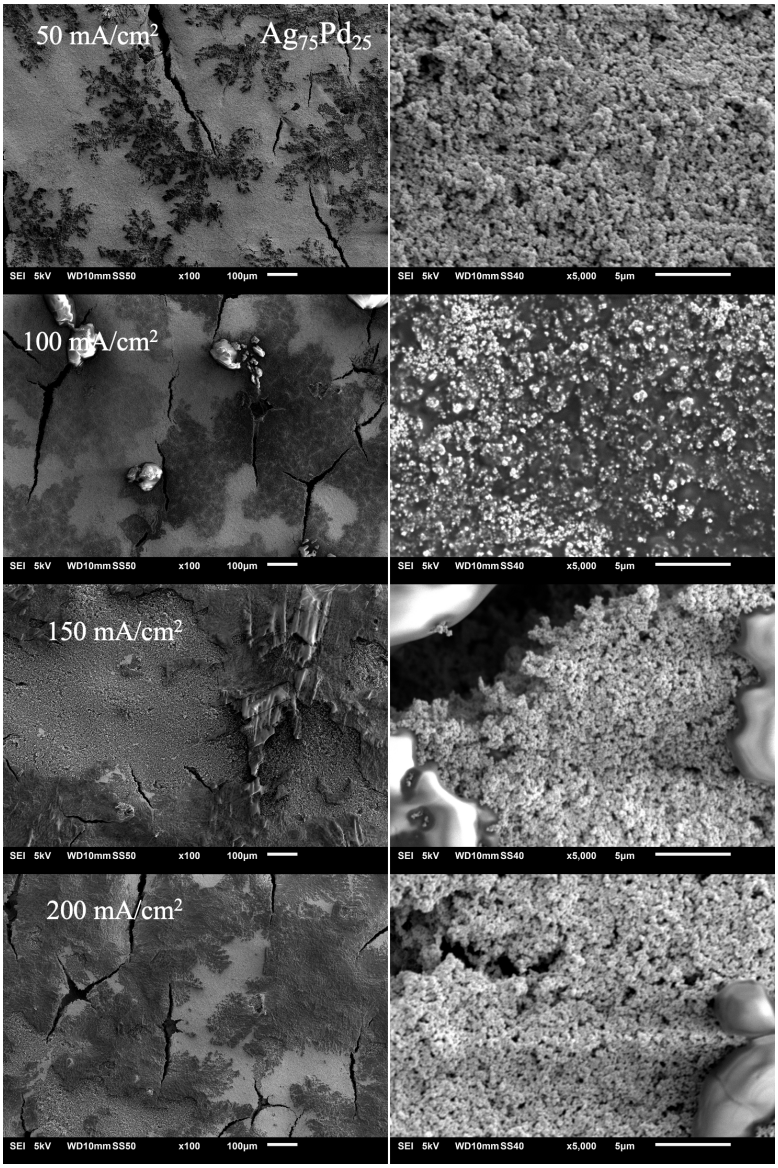

Figure C.7: *SEM images of the $Ag_{75}Pd_{25}$ surface after electrolysis at the different current densities.*

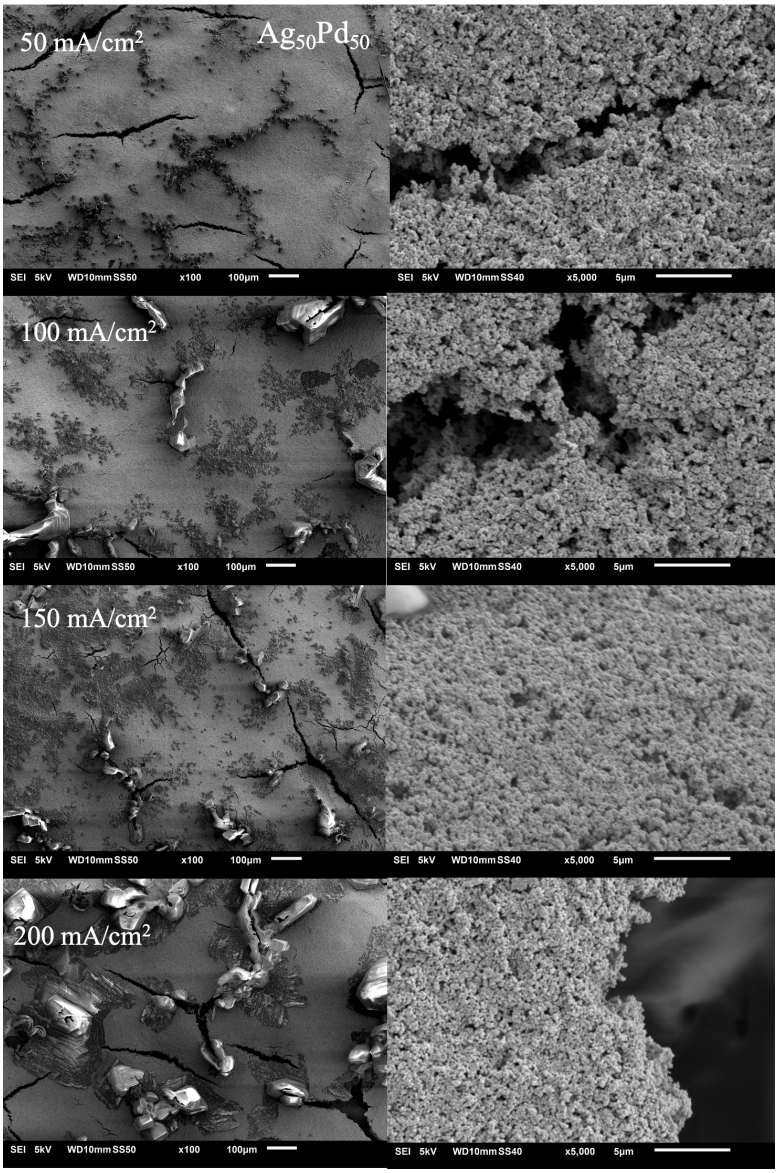

Figure C.8: *SEM images of the $Ag_{50}Pd_{50}$ surface after electrolysis at the different current densities.*

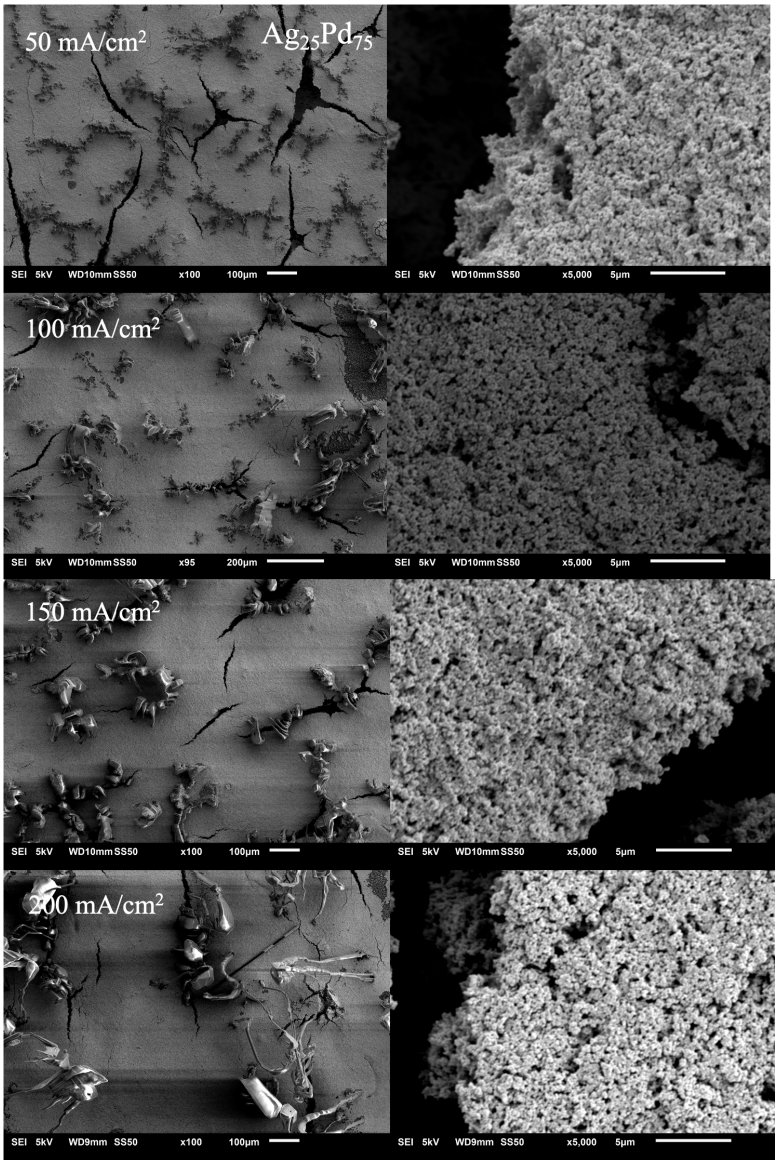

Figure C.9: *SEM images of the $Ag_{25}Pd_{75}$ surface after electrolysis at the different current densities.*

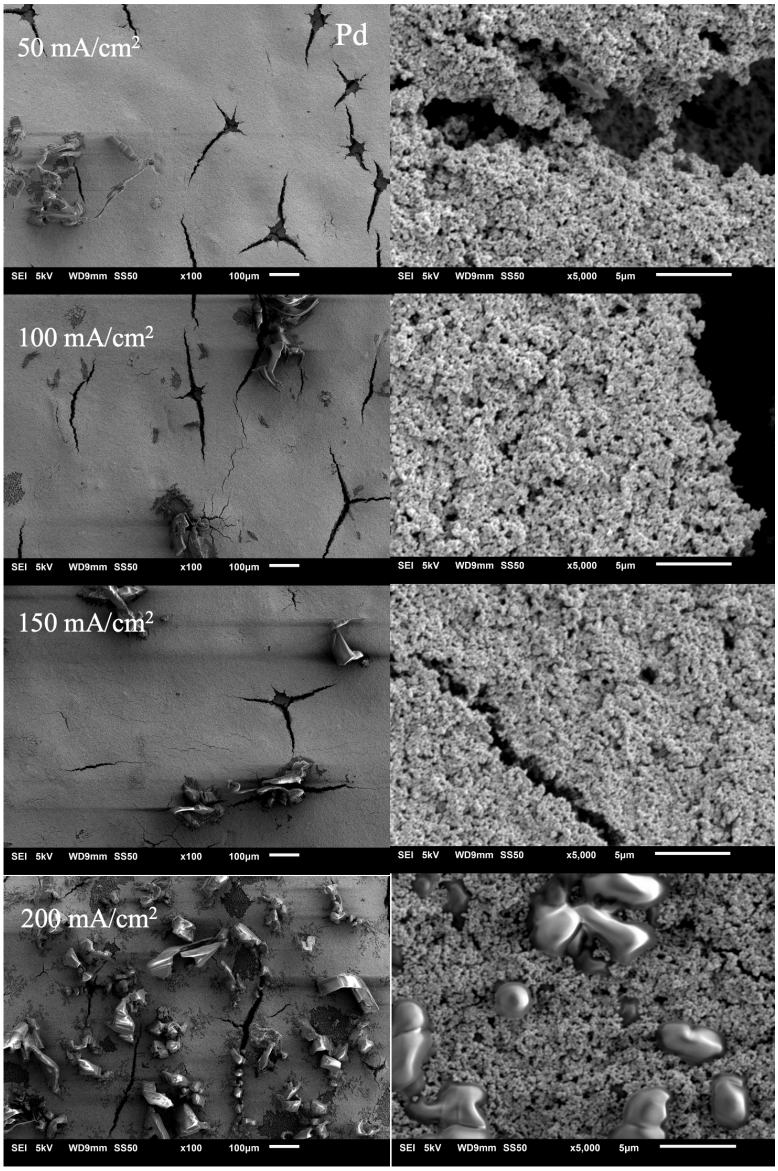

Figure C.10: *SEM images of the Pd surface after electrolysis at the different current densities.*

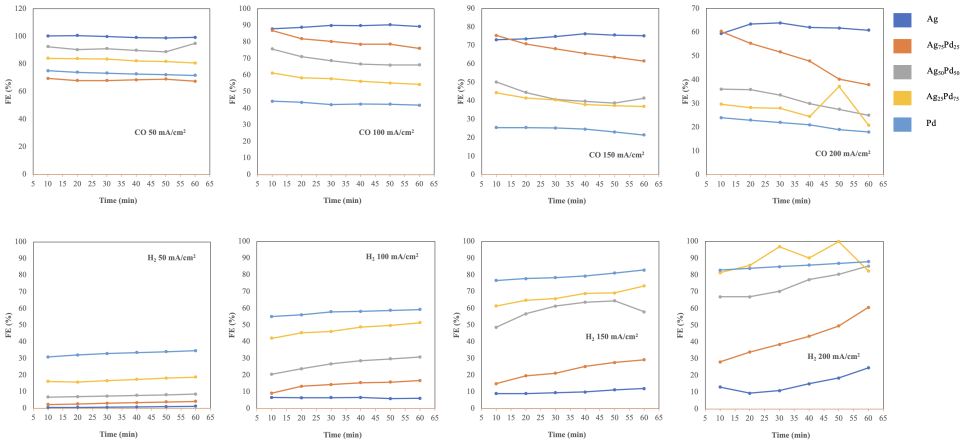

Figure C.11: *Changes in Selectivity of CO and H_2 over 60 minutes.*

CURRICULUM VITÆ

Sanjana CHANDRASHEKAR

21-05-1992 Born in Kolar, Karnataka, India.

EDUCATION

2010–2014 Bachelors in Chemical Engineering
M.S Ramaiah Institute of Technology, Bangalore, India

2014–2015 Research Assistant
Centre for Sustainable Technologies
Indian Institute of Science, Bangalore, India

2015–2017 MSc in Chemical Product Engineering
Faculty of Applied Sciences
Technical University of Delft

2017–2021 PhD. Chemical Engineering
Faculty of Applied Sciences
Technical University of Delft
Thesis: From Small scale to Large Scale in the world of CO_2 Reduction
Promotors: dr. W.A. Smith and dr. J.J.C. Geerlings

LIST OF PUBLICATIONS

8. Sassenburg, M.; Rooij, R. De; Nesbitt, N. T.; Kas, R.; **Chandrashekar**, S.; Firet, N. J.; Yang, K.; Liu, K.; Blommaert, M. A.; Kolen, M.; Ripepi, D.; Smith, W. A.; Burdyny, T. *Ċharacterizing CO 2 Reduction Catalysts on Gas Di Ff Usion Electrodes: Comparing Activity, Selectivity, and Stability of Transition Metal Catalysts*, ACS Appl. Energy Mater. **2022**, 5, 5, 5983–5994.

7. **Chandrashekar**, S.; Geerlings, H.; Smith, W. A. Assessing Silver Palladium Alloys for Electrochemical CO $_2$ Reduction in Membrane Electrode Assemblies. ChemElectroChem **2021**, 8, 4515–4521.

6. Feleki, B. T.; **Chandrashekar, S.**; Bouwer, R. K. M.; Wienk, M. M.; Janssen, R. A. J. , *Ďevelopment of a Perovskite Solar Cell Architecture for Opaque Substrates.*, Sol. RRL **2020**.

5. **Chandrashekar, S.**; Nesbitt, N. T.; Smith, W. A., *Ëlectrochemical CO2Reduction over Bimetallic Au-Sn Thin Films: Comparing Activity and Selectivity against Morphological, Compositional, and Electronic Differences*, J. Phys. Chem. C **2020**, 124 (27), 14573–14580.

4. Firet, N. J.; Burdyny, T.; Nesbitt, N. T.; **Chandrashekar, S.**; Longo, A.; Smith, W. A., *Ċopper and Silver Gas Diffusion Electrodes Performing CO2reduction Studied through: Operando X-Ray Absorption Spectroscopy*, Catal. Sci. Techno **2020**, 10 (17), 5870–5885).

3. Hutter, E. M.; Sutton, R. J.; **Chandrashekar, S.**; Abdi-Jalebi, M.; Stranks, S. D.; Snaith, H. J.; Savenije, T. J., *V̈apour-Deposited Cesium Lead Iodide Perovskites: Microsecond Charge Carrier Lifetimes and Enhanced Photovoltaic Performance*, ACS Energy Letters **2017**, 2 (8)2 (1901–1908).

2. Khuntia, H. K.; **Chandrashekar, S.**; Chanakya,H.N *T̈reatment of Household Greywater Laden with Household Chemical Products in a Multi-Chambered Anaerobic Biofilm Reactor.*, Sustain. Cities Soc **2019**, 51 (December 2018), 101783.

1. Bhat, A.; Megeri, G. B.; Thomas, C.; Bhargava, H.; Jeevitha, C.; **Chandrashekar, S.**; Madhu, G. M., *Ädsorption and Optimization Studies of Lead from Aqueous Solution Using -Alumina.*, J. Environ. Chem. Eng. **2015**, 3 (1), (30–39).